Faculty of Aerospace Engineering

Interval Based Integer Ambiguity Resolution Using Multiple Antennas

Applied to airplane attitude determination

M. Zemowski B.Sc.

August 16, 2011

TU Delft Delft University of Technology

Challenge the future

Interval Based Integer Ambiguity Resolution Using Multiple Antennas

Applied to airplane attitude determination

Master of Science Thesis

M. Zemowski B.Sc.

August 16, 2011

Faculty of Aerospace Engineering · Delft University of Technology

Delft University of Technology

Delft University Of Technology
Department Of
Control and Simulation

The undersigned hereby certify that they have read and recommend to the Faculty of Aerospace Engineering for acceptance a thesis entitled **"Interval Based Integer Ambiguity Resolution Using Multiple Antennas"** by **M. Zemowski B.Sc.** in partial fulfillment of the requirements for the degree of **Master of Science**.

Dated: August 16, 2011

Readers:

prof.dr.ir. M. Mulder

dr.ir. E. van Kampen

dr.ir. Q. P. Chu

Abstract

Finding the correct integers is the key to high precision range measurements. This has been an issue of investigation since the early 1980's and many different techniques have been developed, none of them can guarantee to resolve the correct integers in 100% of the cases (Kim & Langley, 2000) though. This thesis focuses on a new approach for Integer Ambiguity Resolution (IAR), using a geometric approach and Interval Analysis (IA). The new method can guarantee that if all measurement errors are bounded by the interval bands the correct integers will always be found. Depending on the width of the interval bands though, there may be more than one solution.

The research objective of the thesis is to determine if the Interval Based Integer Ambiguity Resolution (IBIAR) method can be used for accurate attitude determination with only one remaining (correct) solution. Earlier results using the Bounded integer ambiguity resolution using interval analysis (BOUNDS) algorithm (van Kampen, 2010) have shown that one solution can not be obtained for all epochs when applied to flight data from a Cessna Citation II research airplane equipped with three antennas. The analysis did not make use of two frequencies, comparing the baseline orientations and adding an extra antenna though. These aspects are added to the BOUNDS algorithm in order to potentially reduce the number of solutions. Further the effects of the noise on both the carrier phase measurements and baseline lengths are investigated.

All simulations are done off line as no real flight data is available for the test configurations. The simulations are loosely based on the Cessna Citation II research airplane belonging to the Dutch National Aerospace Laboratory (NLR) and Delft University of Technology (DUT). For all simulations the correct solution is bounded by the noise levels, which means that the BOUNDS algorithm theoretically always finds the correct solution. Further it is assumed that there are no multipath effects, no restrictions on the attitude angles the airplane can fly with, that the antennas always have a clear view of the satellites and the cut off angle is zero degrees.

The conclusion of the thesis is that the IBIAR method can be used for attitude de-

termination where one (correct) solution remains but the accuracy of the solution is low. The thesis gives recommendations on how to improve the accuracy of the attitude angles.

Acknowledgments

I would like to thank my supervisor dr.ir. E. van Kampen for his assistance during the thesis. At the beginning of the thesis he suggested me reading the book of R. E. Moore on IA, which together with his PHD dissertation gave me a new insight to optimization.

I would also like to thank prof.dr.ir. M. Mulder for the inspiring environment I am working in at the Control & Simulation (C&S) department and my home university KTH Royal Institute of Technology (KTH) for making it possible to do my thesis abroad.

Further I would like to thank all the people I meet on ERASMUS for their support during the thesis. A special thanks goes to V. Alvarez and E. Lundeberg for the feedback they gave me on the thesis. And last but not least I would like to than my mother, father and brother for always being there for me.

Delft, University of Technology — Mikael Zemowski B.Sc.
August 16, 2011

Contents

List of Figures

List of Tables

Nomenclature

Greek Symbols

α	Cone angle between the baseline vector and the line of sight vector to the satellite
β	Angle between two satellite line of sight vectors
δ	Azimuth angle of circle intersection point
δt	Clock bias
Δ	Correction term for long baselines
ε	Mesurment error
θ	Pitch angle
λ	Wavelength
λ_{long}	Longitude
ρ	Pseudorange
τ	Transit time
ϕ	Carrier phase observation
Φ	Carrier phase observation multiplied by wavelength
φ	Bank angle
φ_{glat}	Geocentrical latitude
ψ	Heading angle
ω	Angle between local and global x-axis

Roman Symbols

$\mathbf{b}$	Baseline vector
c	Speed of light
$\mathbf{e}$	Line of sight vector
f	Frequency
F	Reference frame
i	Intersection point
I	Ionospheric delay
N	Integer ambiguity
n_{sat}	Number of satellites in view
r	Receiver

R	Rotation matrix
s	Satellite
T	Tropospheric delay
$\mathbf{T}$	Transformation matrix
t	Time
t_0	Time at start of observation
$[x]$	Interval notation for variable x
Z	Projection of an α-band onto the line of sight vector

Subscripts

i	Refers to receiver i
ij	Difference between receiver i and j
r	Receiver

Superscripts

a	Antenna
b	Body
p	Refers to satellite p
pq	Difference between satellites p and q
pQ	Global reference frame
s	Satellite
$*$	Second intersection point

Acronyms

AFM	Ambiguity Function Method
C&S	Control & Simulation
BF	Body Fixed
BOUNDS	Bounded integer ambiguity resolution using interval analysis
C/A	Coarse/Acquisition
CBO	Compared Baseline Orientation
DD	Double Differencing
DUT	Delft University of Technology
ECEF	Earth Centered Earth Fixed
GLONASS	GLObalnaja NAvigatsionnaja Sputnikovaja Sistema
GNSS	Global Navigation Satellite System
GPS	Global Positioning System
IA	Interval Analysis
IAR	Integer Ambiguity Resolution
IBIAR	Interval Based Integer Ambiguity Resolution
ILS	Integer Least-Squares
INTLAB	INTerval LABoratory
KTH	KTH Royal Institute of Technology
LAMBDA	Least-squares AMbiguity Decorrelation Adjustments
MATLAB	MATrix LABratory
NANU	Notice Advisory to NAVSTAR Users
NAVSTAT GPS	NAVigation Signal Timing And Ranging Global Positioning System
NCBO	Not Compared Baseline Orientation
NED	North-East-Down
NLR	Dutch National Aerospace Laboratory
PRN	Pseudo Random Noise
RAAN	Right Ascension of the Ascending Node
SBAS	Space Based Augmentation Systems
SD	Single Differencing
UAV	Unmanned Aerial Vehicle

WGS 84 World Geodetic System 1984

Chapter 1

Introduction

The usage of the GNSS has increased rapidly over the last decades, and it is nowadays used widely for both civil and military applications. The main systems are GPS and GLObalnaja NAvigatsionnaja Sputnikovaja Sistema (GLONASS) developed by USA and Russia respectively. The Europeans and Chines are currently developing two similar systems, GALILEO and COMPASS which are suppose to be operational within ten years (European Space Agency, 2011),(Inside GNSS, 2011).

These systems can provide a receiver with three different measurements, pseudorange, Doppler shift and carrier phase measurements. The GPS pseudorange measurements can provide an accuracy of around one meter when used with proper Space Based Augmentation Systems (SBAS) and the antenna is close to an reference station (Ventura-Traveset, Gauthier, Toran, de Lesthievent, & Bedu, 2005) (Eldredge, 2011). The Doppler shift measurement are useful when determining the velocity of an moving vehicle but the velocities need to be very high (Hofmann-Wellenhof, Lichtenegger, & Collins, 2001). The carrier phase measurements can give an position accuracy in the millimeter range but the integer ambiguities need to be resolved.

This has been an issue for investigations since the early 1980's (Kim & Langley, 2000) and several methods have been proposed. The most widely used is the Least-squares AMbiguity Decorrelation Adjustments (LAMBDA) technique developed at the DUT in the mid 1990's (Teunissen, 1995). The thesis will focuses on a new approach using the IBIAR (de Weerdt, van Kampen, Chu, & Mulder, 2008) though.

This method uses the BOUNDS algorithm to determine the integer ambiguities between two receivers. The algorithm can guarantee that the correct solution will be found if all errors are bounded by the interval bands. Depending on the width of the error interval bands though, there may be more than one solution. The algorithm can be applied for high accuracy attitude determinations, such as Unmanned Aerial Vehicle (UAV), landing systems for aircraft, military aircraft and space applications (van Kampen, de Weerdt, Chu, & Mulder, 2009).

The attitude of a vehicle is its orientation with respect to a defined frame of reference. This in an aircraft is denoted by the pitch, heading and bank angles, which are given with respect to the defined North-East-Down (NED) reference frame. The angles are usually determined using gyros today and although the obtained accuracy can be very high, the systems are very expensive (Barbour & Schmidt, 2001).

1-1 Research Objectives and Structure of the thesis

The research objective of the thesis is to determine if the IBIAR method can be used for accurate attitude determination where only one (correct) solution remain. Earlier results using the BOUNDS algorithm (van Kampen, 2010) have shown that one solution can not be obtained for all epochs when applied to flight data from a Cessna Citation II research airplane equipped with three antennas. The analysis did not make use of two frequencies, comparing the baseline orientations and adding an extra antenna though. The four main investigations are therefore:

1. The effects of comparing the baseline orientations as they are known in the Body Fixed (BF) reference frame.
2. The effects of adding an extra antenna and frequency (L2 for GPS).
3. The effects of the noise on the carrier phase measurements.
4. The effects of the noise on the baseline lengths.

Chapters 2 to 5 cover the theoretical background of the thesis. It is recommended that the reader has some basic knowledge of GNSS and IA as these are only briefly introduced in Chapter 2 and 3. Chapter 4 presents previous methods for solving the IAR and thoroughly describes the IBIAR method. In Chapter 5 it is described how the attitude of an aircraft is obtained from multiple antennas and the IBIAR method. It is also explained how gyroscopes are used for attitude determination nowadays.

The second part of the thesis implements the BOUNDS algorithm to simulated carrier phase measurements. In Chapter 6 the experimental setup of the four investigations are explained in detail. In Chapter 7 the main results of the investigations are given and Chapter 8 and 9 concludes the thesis and gives recommendations. All results of the simulations are tabulated in Appendix C.

Part I

Theory

Chapter 2

Global Navigation Satellite System

The art of millimeter-accuracy positioning and navigation has taken the human kind nearly two thousands years to develop and started by the ancient Greeks. The three main fields of development to this goal where geodesy, timekeeping and astronautics (Misra & Enge, 2006).

Geodesy, which started with the ancient Greeks developing a coordinate system and defining the equator and the poles all the way to the colonization in the sixteenth and seventeenth century which gave birth to mapping of the earth. The giant leaps in technology of clock making and astronautics where fueled by the cold war and moon race. This ended in the development of the GPS by the USA and GLONASS by the former Soviet Union.

This Chapter gives a short introduction to the GPS as the carrier phase measurements will be used in Chapter 4 and the measurement simulator is based on the GPS. Most of the material is taken from (Misra & Enge, 2006) and (Kaplan & Hegarty, 2006), the author highly recommends these books for those with no previous knowledge of GNSS.

2-1 Global Positioning System Principle

The true name is NAVigation Signal Timing And Ranging Global Positioning System (NAVSTAR GPS) and it was fully operational in 1995. The system is available for a unlimited number of users for land, air and space applications. All that is needed is a receiver and for many applications the position can be obtained nearly instantaneously.

The basic principle of the GPS is illustrated in Figure 2-1 (Misra & Enge, 2006). Each satellites will send out a specific Pseudo Random Noise (PRN) code sequence and navigation message imprinted on a carrier wave signal. The receiver can than read out the position $\left(x^{(k)}, y^{(k)}, z^{(k)}\right)$ and transit time τ from the signal. The unknowns are the receiver (x, y, z) position and clock biases δt. Assuming that the signal will travel with the speed of

light c, the pseudorange measurements ρ are:

$$\begin{aligned}\rho^{(k)} &= c\tau - \delta t \\ &= \sqrt{\left(x^{(k)} - x\right)^2 + \left(y^{(k)} - y\right)^2 + \left(z^{(k)} - z\right)^2} - \delta t \\ k &= 1,\, 2,\, ...,\, K\end{aligned} \tag{2-1}$$

If four or more satellites are in view the position of the receiver can be determined.

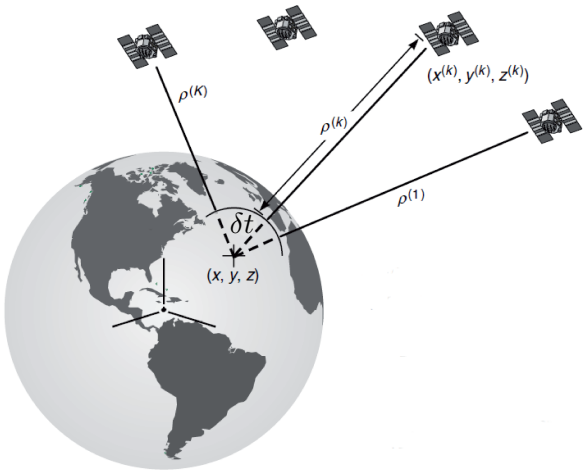

Figure 2-1: The principle of GNSS position determination.

2-1-1 Satellite Geometry

The nominal GPS consisted of 24 satellites and currently there is around 32 in orbit around the earth (Notice Advisory to NAVSTAR Users, 2011), distributed over 6 orbital planes at an inclination of 55° to the equator. The orbits are nearly circular with a radius of around 26650 km and the orbital period is 11 hours and 58 minutes, which means that the satellite makes two revolutions in one sidereal day (in one sidereal day the earth makes exactly one revolution around its axis). The number of satellites in view at any location is usually between $5-10$, although this will vary with geographical position and elevation cut-off angle of receiver.

The Notice Advisory to NAVSTAR Users (NANU) is in charge of maintains and monitoring of the satellites. The main objectives of the control segment are to:

- Monitor satellite orbits.
- Monitor and maintain satellite health.
- Predict satellite ephemeris and clock parameters.
- Command maneuvers/relocations of satellites.

Ephemeris is the position (in the World Geodetic System 1984 (WGS 84) coordinate frame) of the satellite. The clock parameters include the offset and drift of the rubidium clocks used in the satellites that need to be predicted with nanosecond precision. The information from NANU is imprinted onto the satellite navigation messages.

2-1-2 Signal Components

All signal components are derived from the fundamental frequency $f_0 = 10.23$ MHz and Figure 2-2 shows a block diagram of the different components. The GPS uses two carrier wave frequencies, the L1 and L2 with a wavelength of 19.05 and 24.45 cm respectively.

On the L1 carrier wave the Coarse/Acquisition (C/A) and P(Y) codes are modulated and on the L2 only the P(Y) code. The C/A code is an unclassified PRN sequence unique for each satellite, with a chipping rate of 1.023 MHz. Each chip has a wavelength of 293.1 meters and the maximum resolution of the wavelength is 0.1–1 % (0.3–3 m). The P(Y) code is the sum of a P and W code. The first being a very long (266 days compared to C/A ~ 1 millisecond) unclassified PRN code with a chip wavelength of 29.31 m, it can be resolved with a accuracy of 0.3–1 % (10–30 cm). The W code is a much shorter encrypted code sequence enabled by the US military in 1994 which makes it very hard to align the P(Y) code with the one generated by the receiver. The satellite navigation message is broadcasted on the L1 carrier-wave with 50 bits per second and contains information from the control segment, a full message is 12.5 minutes long.

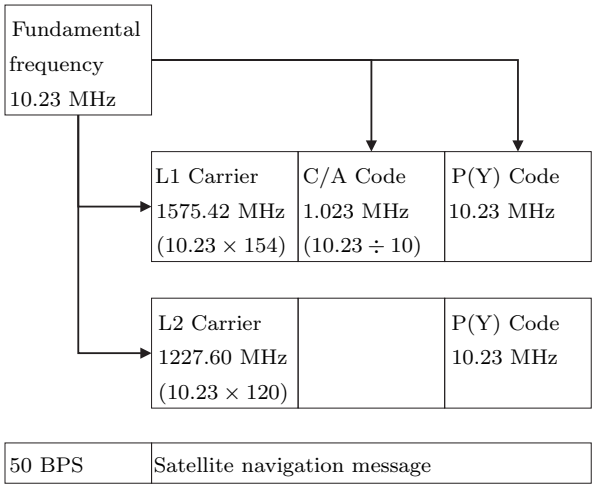

Figure 2-2: GPS signal components.

2-1-3 Receivers

The signal from the satellites is very week, for on land application the signal to noise ratio is around 1/80. The antenna will therefore amplify the signal, then the receiver will generate a replica of the satellite signal, which is well known for the C/A code. It will align the sequences, which is easy as the PRN code is highly uncorrelated. Once the satellite and receiver generated signal are aligned the receiver can read out the ephemeris, clock parameters and transit time from the satellite navigation message. For the P(Y) code this is much harder as it contains the encrypted code sequence W, which makes it difficult to align it with the receiver generated P code.

Another option is to use the phase observation of the L1 and L2 carrier waves to

measure the phase difference between the satellite generated and receiver generated sine wave. The only problem being that the number of cycles is unknown, the integer ambiguity.

2-1-4 Error Sources

The four main error sources are the satellite clock/ephemeris, atmospheric propagation estimations, receiver noise and multipath. The clock and ephemeris errors are due to the fact that the control segment can only measure the clock offsets and ephemeris to a certain accuracy. If these parameter errors are major the control segment can transmit through the satellite navigation message that the satellite should not be used. The atmospheric propagation errors are due to time delays when the signal travels through the troposphere and ionosphere. The signal will not travel at the same velocity in vacuum as in the ionosphere for example. Time delays can be modeled and the accuracy will depend on which method is used. The main

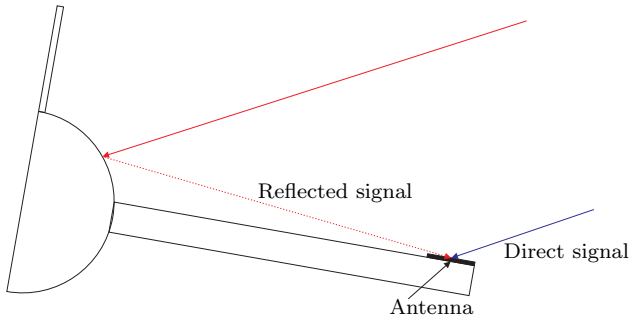

Figure 2-3: Multipath of satellite signal for wing placed antenna.

error sources in attitude determination are the receiver noise and multipath. The noise of the receiver will depend on choice of antenna receiver configuration, and the placement of the receiver. The multipath error is the hardest to deal with, Figure 2-3 shows the problem with wing placed antennas on airplanes. The antenna can receive two signal, one with an apparent longer range than the other. A way to deal with multipath errors is choke rings, which are not ideal from an aerodynamic type of view or to increase the cut off angle which will reduce the number of satellites in view. Another way is trying to model them, this may be very hard when using carrier phase measurements as the multipath errors would need to be predicted with millimeter accuracy. For modern airplanes the multipath errors for wing placed antennas may be even larger as the wingtips are often bended, introducing one extra multipath.

2-1-5 Other Global Navigation Satellite Systems

There is currently three other major GNSS in use or under development. The Russian GLONASS developed around the same time as GPS with the main difference being that it has 3 orbital planes at a much higher inclination, this to have better coverage over Russia. The other two systems under development are the European GALILEO and Chinese COMPASS (also known as BeiDou-2). The differences compared to the GPS are that they will send more signals on different frequencies and that they will have a different satellite

configuration to give optimal coverage over Europe and China. The European system should be fully functional around 2014 and the Chinese in 2020.

2-2 Carrier Phase Measurements

Using the L1 and L2 carrier phase measurements to determine the pseudorange leads to an position accuracy in the millimeter level if the integer ambiguity is resolved, the methods for solving this will be presented in Chapter 4. The carrier phase measurement is the difference in phase of the satellite and receiver generated carrier wave (on the L1 and L2 frequency for the GPS). Figure 2-4 illustrates the carrier phase measurement ϕ. The carrier phase range

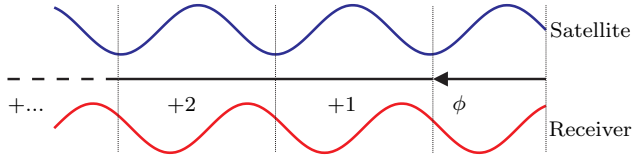

Figure 2-4: Receiver and satellite generated signal.

(in terms of cycles) as a function of time t is:

$$\phi(t) = \phi_r(t) - \phi^s(t-\tau) + N + \varepsilon_\phi \tag{2-2}$$

where subscript $(\bullet)_r$ is for receiver, superscript $(\bullet)^s$ for satellite, N is the unknown number of integer and ε_ϕ all other errors. Equations 2-3 and 2-4 are the carrier phases of the satellite and receiver where t_0 is the time at start of observation, f is the frequencies and δt the clock bias.

$$\phi_r(t) = \phi_r(t_0) + f \cdot (t - t_0) + f \cdot (\delta t_r(t) - \delta t_r(t_0)) \tag{2-3}$$

$$\phi^s(t-\tau) = \phi^s(t_0) + f \cdot (t - \tau - t_0) + f \cdot (\delta t^s(t-\tau) - \delta t^s(t_0)) \tag{2-4}$$

Equation 2-2 can be rewritten when inserting Equations 2-3 and 2-4. Further if it is multiplied with the wavelength λ to get the carrier phase range Φ in meters, where $(\bullet)_r^s$ stands for the difference between satellite and receiver, I is the ionospheric delay, T is the tropospheric delay and ε_Φ all other errors in meters.

$$\begin{aligned}\Phi(t) = \rho_r^s - I_r^s + T_r^s + c \cdot (\delta t_r(t) - \delta t^s(t-\tau)) + \lambda \cdot (\phi_r(t_0) - \phi^s(t_0)) - \\ c \cdot (\delta t_r(t_0) - \delta t^s(t_0)) + \lambda N + \varepsilon_\Phi\end{aligned} \tag{2-5}$$

2-2-1 Single and Double Differencing

To obtain millimeter accuracy many parameters must be correctly estimated in Equation 2-5, many of these will cancel out when using SD and Double Differencing (DD). The SD Equation 2-6 is obtained when subtracting observations from receiver i to j to the same satellite p at the same time instance ($(\bullet)_{ij} = (\bullet)_i - (\bullet)_j$). When subtracting the SD equation from satellite p to q (at the same time instance) the DD Equation 2-7 is obtained ($(\bullet)_{ij}^{pq} = (\bullet)_{ij}^p - (\bullet)_{ij}^q$).

$$\Phi_{ij}^p(t) = \rho_{ij}^p - I_{ij}^p + T_{ij}^p + c\delta t_{ij}(t) + \lambda\phi_{ij}(t_0) - c\delta t_{ij}(t_0) + \lambda N_{ij}^p + \varepsilon_{\Phi,ij}^p \tag{2-6}$$

$$\Phi_{ij}^{pq}(t) = \rho_{ij}^{pq} - I_{ij}^{pq} + T_{ij}^{pq} + \lambda N_{ij}^{pq} + \varepsilon_{\Phi,ij}^{pq} \tag{2-7}$$

Chapter 3

Interval Analysis

In 1962 R.E. Moore completed his dissertation in the field of Numerical Errors in Computing and four years later he published the book *Interval Analysis*, which is the reference of IA to this day (Jaulin, Kieffer, Didrit, & Walter, 2001). For the first 20 years the field remained very confined to the University of Karlsruche and its researchers, where R.E Moore finished his dissertation.

In the 1990's the field grew larger and in 1991 it got it's own magazine, *Interval Computations*, later renamed to *Reliable Computing*. Several international conferences are held on the subject nowadays and thousands of papers on the subject can be found on the website of Computer Science Bibliography (Computer Science Bibliography, 2011).

This chapter gives a short introduction to the interval numbers and arithmetics of importance for the thesis. The last section of the chapter gives an simple optimization example showing the strength of IA. The book *Interval Analysis* (Moore, Baker Kearfoot, & Cloud, 1966) is highly recommended as an introduction to IA, the PHD dissertation *Global Optimization using Interval Analysis* (van Kampen, 2010) for understanding of interval optimization algorithm and the book *Applied Interval Analysis* (Jaulin et al., 2001) for applications of IA. The environment used for computations is INTerval LABoratory (INTLAB), a package for MATrix LABratory (MATLAB) developed by S. Rump at the Institute of Reliable Computing at the Technical University of Hamburg (Rump, 2011)

3-1 Numbers and Arithmetics

A closed interval $[x]$ is a set of numbers given by (Moore et al., 1966):

$$[a, b] = \{x \in \mathbb{R} \mid a \leq x \leq b\} \tag{3-1}$$

where a and b are the lower and upper bound of the interval, both real numbers. The bounds are returned by the infinum and supreum operators:

$$\inf([x]) = a \tag{3-2}$$
$$\sup([x]) = b \tag{3-3}$$

Further the width, midpoint and absolute value of $[x]$ are:

$$w([x]) = \sup([x]) - \inf([x]) \tag{3-4}$$
$$m([x]) = \frac{1}{2} \cdot (\sup([x]) - \inf([x])) \tag{3-5}$$
$$\|[x]\| = \max(\inf([x])), \sup([x]) \tag{3-6}$$

3-1-1 Arithmetic Operations

The four basic operations addition, subtraction, multiplication and division between the intervals $[x] = [a, b]$ and $[y] = [c, d]$ are defined as:

$$[x] + [y] = [a + c, b + d] \tag{3-7}$$
$$[x] - [y] = [a - d, b - c] \tag{3-8}$$
$$[x] \cdot [y] = [\min(ac, ad, bc, bd), \max(ac, ad, bc, bd)] \tag{3-9}$$
$$[x] \div [y] = [a, b] \cdot [1 \div d, 1 \div c] \quad \text{if } 0 \notin [y] \tag{3-10}$$

Further addition and multiplication is both associative and communitive:

$$([x] + [y]) + [z] = [x] + ([y] + [z]) \tag{3-11}$$
$$([x] \cdot [y]) \cdot [z] = [x] \cdot ([y] \cdot [z]) \tag{3-12}$$
$$[x] + [y] = [y] + [x] \tag{3-13}$$
$$[x] \cdot [y] = [y] \cdot [x] \tag{3-14}$$

In interval arithmetics the distributive law does not hold:

$$[x] \cdot ([y] + [z]) \neq [x] \cdot [y] + [x] \cdot [z] \tag{3-15}$$

but there is a sub-distributive law:

$$[x] \cdot ([y] + [z]) \subseteq [x] \cdot [y] + [x] \cdot [z] \tag{3-16}$$

The intersection of two intervals will always result in a single new interval (may be empty), defined as:

$$[x] \cap [y] = \{z \in \mathbb{R} \mid z \in [x] \text{ and } z \in [y]\} \tag{3-17}$$

and the union of two intervals is defined as:

$$[x] \cup [y] = \{z \in \mathbb{R} \mid z \in [x] \text{ or } z \in [y]\} \tag{3-18}$$

The union of two intervals does not have to consist of a single interval, however the hull of two intervals will result in a single new interval, defined as:

$$[x] \underline{\cup} [y] = [\min(a, c), \max(b, d)] \tag{3-19}$$

3-1-2 Fundamental Theorem of the Interval Analysis

Theorem 3-1-2
If $F([x]_1, ..., [x]_n)$ *is an inclusion isotonic interval extension of* $f(x_1^*, ..., x_n^*)$*, then*

$$f(x_1^*, ..., x_n^*) \subseteq F([x]_1, ..., [x]_n) \tag{3-20}$$

where $(x_1^*, ..., x_n^*) \in ([x]_1, ..., [x]_n)$ (Moore et al., 1966).

All interval operations are based on this central theorem, "which states that the outcome of the operations on a subset of the input interval arguments is included in the outcome of the operations performed on complete input intervals. The subset can be smaller intervals or crisp numbers (thin intervals)" (van Kampen, 2010).

3-1-3 Dependency Problem and Endpoint Analysis

When working with IA dependency reduction and endpoint analysis are two ways of minimizing the width of the intervals. This is best illustrated with an example of the function $f(x) = x^2 - x$ in the range $[x] = [-0.1\ ,\ 0.25]$. The function can be calculated in three ways:

$$[x]^2 - [x] = [-0.2501\,, 0.1626] \tag{3-21}$$

$$[x] \cdot ([x] - 1) = [-0.2751\,, 0.1101] \tag{3-22}$$

$$-.25 + ([x] - .5)^2 = [-0.1876\,, 0.1101] \tag{3-23}$$

The width of the solutions for Equation 3-21 to 3-23 are 0.4125, 0.3850 and 0.2975. When $[x]$ only appears once the arithmetic operations will produce the exact range. This leads to two important observations (Moore et al., 1966):

1. Two rational expressions which are equivalent in real arithmetic may not be equivalent in interval arithmetic.

2. Any natural interval extension of a rational function in which each variable only occurs once (if at all) and to the first power only will compute the exact range of values provided that no division by an interval containing zero occurs.

It is not always possible to reduce the function to contain each variable once and only to the power of one. This can be omitted if using endpoint analysis. This is illustrated by $f(x) = x^2 - x$, for which the derivative $f(x) = 2 \cdot x - 1$ is solely negative in the range $[x] = [-0.1\ ,\ 0.25]$. Performing the computations on Equation 3-21 using $\inf([x])$ and $\sup([x])$ instead and taking the hull of the result will give the same range as Equation 3-23. This leads to one more important observation (van Kampen et al., 2009):

3. The dependency can be eliminated if using endpoint analysis only if the first order derivative with respect to $[x]$ is solely positive or negative for the entire interval.

3-2 Simple Optimization Problem Solved with Interval Analysis

The strength of IA is easiest shown by a simple example, this is the Booth function, illustrated in Figure 3-1. The Booth function is defined accordingly to Equation 3-24, the function has several local minima but only one global minimum with the coordinates $[x_1\,,\,x_2\,,\,Y] = [1\,,\,3\,,\,0]$.

$$Y = (x_1 + 2 \cdot x_2 - 7)^2 + (2 \cdot x_1 + x_2 - 5)^2 \tag{3-24}$$

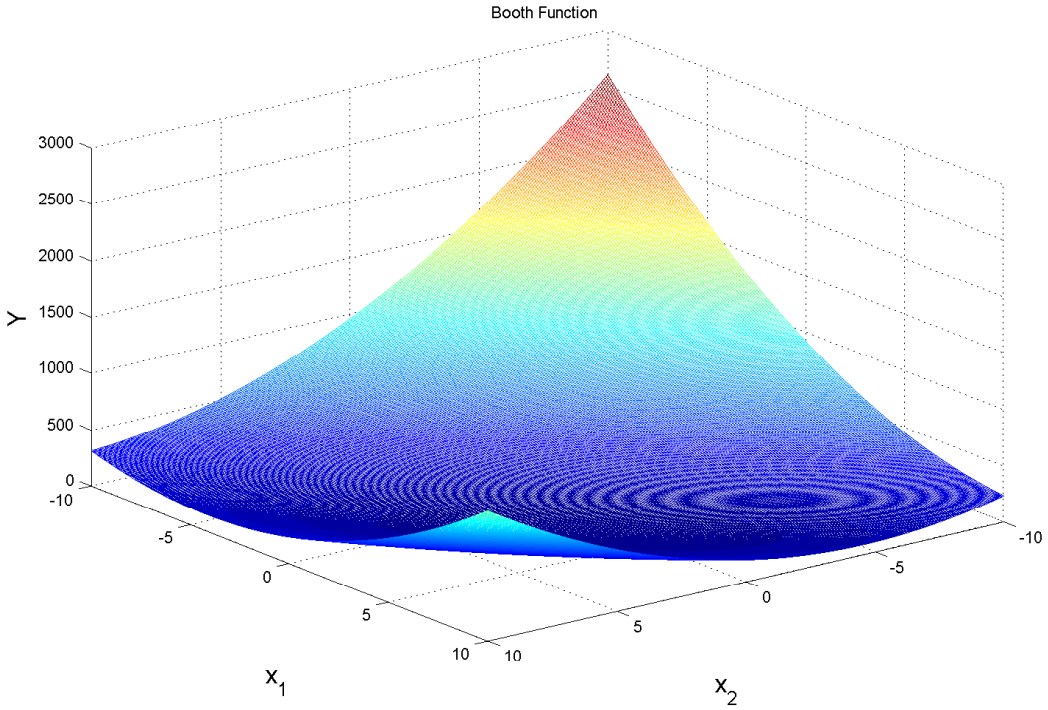

Figure 3-1: The Booth function with several local minima but only one global minimum at $[x_1\,,\,x_2\,,\,Y] = [1\,,\,3\,,\,0]$.

The function is nonlinear and finding the optimal solution (minimum in this case) is usually done with gradient based methods, amongst them the most known is Newton's method. These method use an initial start guess to find the global minimum, with the problem being that they might not find the correct solution. This is illustrated by the Booth function where the gradient based methods can very easily get stuck in a local minimum if the initial start guess is chosen wrongly.

The global minimum of the Booth function may also be found with the interval branch and bound (optimization) algorithm, which can guarantee to find the correct interval solution if it is bounded by the initial search space. First the Booth function is redefined as

$$[Y] = ([x_1] + 2 \cdot [x_2] - 7)^2 + (2 \cdot [x_1] + [x_2] - 5)^2 \tag{3-25}$$

which is an inclusion isotonic interval extension of Equation 3-1 (Theorem 3-1-2). This is an strength when working with IA, as the intervals may be divided into subintervals.

The interval branch and bound (optimization) algorithm starts by defining an initial search space $[[x_1], [x_2]]$. The cost function $[Y]$ is then evaluated from Equation 3-25 and the min value is chosen as $Y_{\min} = \sup([Y])$. After this the Algorithm enters a loop with a stopping criteria that all widths of the intervals $[[x_1], [x_2]]$ need to be smaller than a defined number.

In the first part of the loop $[[x_1], [x_2]]$ are bisected into sub intervals. This is done in a way where the variable $[x_1]$ or $[x_2]$ with the widest interval is bisected into two new intervals. Then the new cost function $[Y]$ is evaluated for the new intervals $[[x_1], [x_2]]$ which are included in the outcome of the operations performed on the initial search space accordingly to Theorem 3-1-2. After this a possible new $Y_{\min} = \sup([Y])$ is found from all the sub intervals. In the last step of the algorithm all sub intervals $[[x_1], [x_2]]$ for which $\inf([Y]) > Y_{\min}$ are deleted. The schematic flowchart of the interval branch and bound algorithm for the Booth function is illustrated in Figure 3-2. Once all intervals are smaller than the specified the correct $[[x_1], [x_2]]$ intervals are extracted.

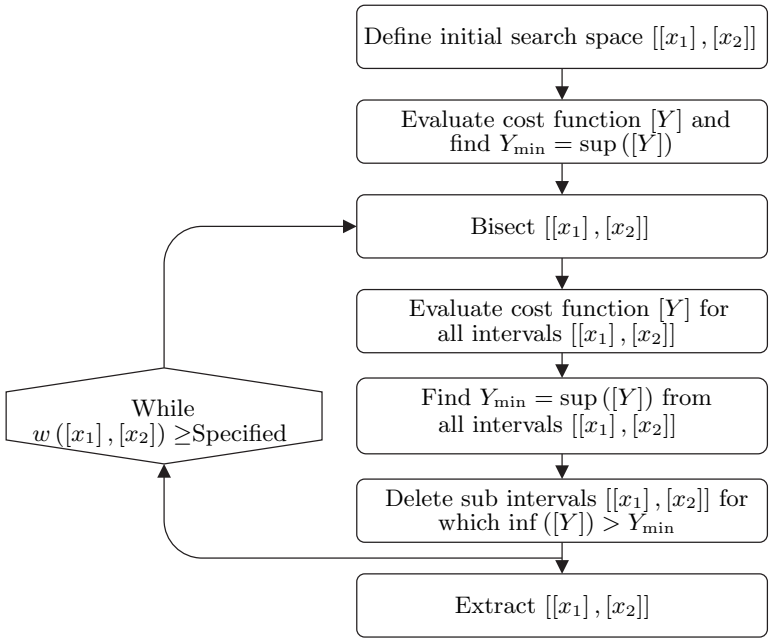

Figure 3-2: Schematic flowchart of the interval branch and bound algorithm for the Booth function.

The interval branch and bound (optimization) algorithm for the Booth function is very similar to most other optimization problems, among them the IBIAR algorithm presented in Chapter 4. Further in Table 3-1 the computational times are given, with different initial search spaces where the stopping criteria is $w([x_1], [x_2]) \leq 10^{-10}$. It should be noted that the algorithm was not optimized for speed.

Table 3-1: Computational times to find the global minimum of the Booth function using the interval branch and bound (optimization) algorithm with different widths on the initial search space. The stopping criteria is $w([x_1], [x_2]) \leq 10^{-10}$.

$[x_1]$	$[x_2]$	$w([x_1], [x_2])$	Computation Time [s]
$[-5, 5]$	$[-5, 5]$	10^1	11.08
$[-50, 50]$	$[-50, 50]$	10^2	12.83
$[-500, 500]$	$[-500, 500]$	10^3	14.42
$[-5000, 5000]$	$[-5000, 5000]$	10^4	15.43
$[-50000, 50000]$	$[-50000, 50000]$	10^5	16.33
$[-500000, 500000]$	$[-500000, 500000]$	10^6	17.94

This example shows the strength of the IA, as the correct solution is always found (if it is bounded by the initial search space). The initial search space can also be extremely large, and still not effect the computational times significantly. This due to that the interval branch and bound algorithm can delete large sub boxes of the initial search space early in computations. Further there will never be a crisp solution but the correct values x_1 and x_2 are bounded by the interval solution $[[x_1], [x_2]]$ (with a width of 10^{-10} in this case).

Chapter 4

Integer Ambiguity Resolution

Finding the correct integers is the key to high precision range measurements. This has been an issue of investigation since the early 1980's and many different techniques have been developed, None of them can guarantee to resolve the correct integers in 100% of the cases (Kim & Langley, 2000) though.

The first section gives a short introduction to previous methods used to find the correct integers and the second section describes the IBIAR in detail. This method uses a geometric approach to solve the IAR problem. It consists of finding the intersections of interval circles that lie on the surface of a sphere. The problem starts from rewriting the SD and DD carrier phase equations and introducing IA to bound all the errors of the measurements. A BOUNDS algorithm is then used to remove combinations of interval circles that do not intersect each other, and thus removing non possible integers. The method finds the relative position between two receivers.

4-1 Previous Methods

The problem of the IAR has received attention from many research groups, and many different techniques have been developed to cope with the problem. These can be divided into three different groups (Kim & Langley, 2000):

1. Ambiguity resolution in the measurement domain.
2. Search techniques in the coordinate domain.
3. Search techniques in the ambiguity domain.

The first group uses the pseudorange measurements computed from the PRN codes, and from these the integer ambiguities are calculated directly. The computational times are very fast but the success rate of obtaining the correct integers is very low as the precision of the

pseudorange measurements are very poor in comparison with the carrier phase measurements. The techniques therefore use linear combinations of the L1 and L2 measurements to increase the success rate. These techniques are usually used in single point positioning, where the accuracy does not have to be in the millimeter range. Many aircraft use these techniques together with the SBAS (Misra & Enge, 2006) for single point positioning, usually during the landing phase. The success rate may then be increased as the SBAS can determine many of the error terms very accurate (mainly the atmospheric delays). These techniques are also suitable for long baseline (> few km) relative positioning where the accuracy may be in the meter range but not for short baselines (meter range accuracy is not adequate). The techniques are therefore not suitable for aircraft attitude determination.

The second group uses a grid search in the coordinate frame to find the correct integers, and include the first technique ever developed to cope with the IAR, namely the Ambiguity Function Method (AFM). Although the AFM has been significantly improved over the years it has relatively poor computational efficiency. Also it can not be guaranteed that the correct solution is found as it may be located between grid points. When the AFM has been applied to relative positioning with baseline lengths ranging from around 1-4 km the average position accuracy has been in the decimeter level, with computational times of around 1-3 seconds (Han & Rizos, 1996). This position accuracy is not good enough for attitude determination and the method is only important out of a historical point of view (Kim & Langley, 2000).

The third group is the most important and involves most of the techniques developed. The LAMBDA method is the most widely used nowadays (Buist, 2007) as it has the guaranteed optimal probability of correct integer estimation (Teunissen, 1999). It is based on the theory of Integer Least-Squares (ILS) (Teunissen, 1995), and integers are obtained in three steps, from the float solution to the integer ambiguity estimation to fixed integer solutions. The main strength of the LAMBDA method is that it computes the integers very fast and can be used for real-time applications. Another strength is that the multi-epoch approach can have a very high success rate of finding the correct integer ambiguities (Kim & Langley, 2000).

The single epoch success rate of finding the correct attitude (integers) of an aircraft based on the baseline constrained LAMBDA method is 58.15% (Buist, 2007). This when the algorithm is applied to data from the Cessna Citation II research airplane (around 3500 epochs) using the L1 carrier phase measurements. If the baseline constrained LAMBDA method is applied to attitude determination of a ship moving in a canal the correct integers are obtained in 99.5% (Buist, 2007). This based on around 9000 epochs of data and single frequency receivers. The main difference between the experimental setup being that the airplane attitude changes faster and the baseline lengths are more dynamic.

4-2 Interval Based Integer Ambiguity Resolution

The BOUNDS algorithm starts by rewriting Equation 2-6 and 2-7. For attitude determination the baselines (distance between receivers) are short and two of the terms of Equation 2-6 can be considered zero, the ionospheric and tropospheric difference terms. They only measure the difference in atmospheric delays between two receivers, and this will not change as the

receivers are very close to each other. Further if the error term is rewritten as:

$$\bar{\varepsilon}^p_{\Phi,ij} = c\delta t_{ij}(t) + \lambda\phi_{ij}(t_0) - c\delta t_{ij}(t_0) + \varepsilon^p_{\Phi,ij} \tag{4-1}$$

the SD and DD equations are rewritten as:

$$\Phi^p_{ij}(t) = \rho^p_{ij} + \lambda N^p_{ij} + \bar{\varepsilon}^p_{\Phi,ij} \tag{4-2}$$

$$\Phi^{pq}_{ij}(t) = \rho^{pq}_{ij} + \lambda N^{pq}_{ij} + \bar{\varepsilon}^{pq}_{\Phi,ij} \tag{4-3}$$

4-2-1 Geometry of the Problem

The geometric visualization of the SD Equation 4-2 is seen in Figure 4-1(a). Here $\mathbf{b}$ is the baseline vector, r stands for the receiver, s for the satellite, $\boldsymbol{\rho}$ is the pseudorange vectors, and Δ is the correction term for long baselines. In Figure 4-1(b) the coordinate frame of the SD Equation 4-2 is defined, where α (cone angle between the baseline vector and the line of sight vector to the satellite) , δ (azimuth angle of circle intersection point) and $\|\mathbf{b}\|$ can determine the position of one receiver with respect to an other. Here $\mathbf{e}$ is the normalized satellite line of sight vector defined as (assumed parallel for both receivers):

$$\mathbf{e}^p_i = \frac{\boldsymbol{\rho}^p_i}{\|\boldsymbol{\rho}^p_i\|} \approx \frac{\boldsymbol{\rho}^p_j}{\left\|\boldsymbol{\rho}^p_j\right\|} = \mathbf{e}^p_j \tag{4-4}$$

From Figure 4-1(a) Equation 4-2 is rewritten:

$$\begin{aligned} \Phi^p_{ij} - \lambda N^p_{ij} - \bar{\varepsilon}^p_{\Phi,ij} &= \rho^p_{ij} \\ &= \mathbf{e}^p_i \cdot \mathbf{b} - \Delta^p_{ij} \\ &= \|\mathbf{e}^p_i\|\,\|\mathbf{b}\|\cos(\alpha^p_{ij}) - \Delta^p_{ij} \end{aligned} \tag{4-5}$$

The term Δ^p_{ij} arises from assuming that $\boldsymbol{\rho}^p_i$ and $\boldsymbol{\rho}^p_j$ are parallel. For baselines shorter than 100 meters this term will be in sub mm level and can be neglected (bounded in the error term). Equation 4-5 then becomes:

$$\Phi^p_{ij} - \lambda N^p_{ij} - \bar{\varepsilon}^p_{\Phi,ij} = \|\mathbf{e}^p_i\|\,\|\mathbf{b}\|\cos(\alpha^p_{ij}) \tag{4-6}$$

and the unknown is the number of integers and each will result in a different α^p_{ij}. The problem is visualized in Figure 4-1(c) where the number of integers change and the baseline can be seen as lying on circles on different planes in a sphere. This visualization is done for each satellite in view in different local reference frame. If these are transformed to the same global reference frame and the error term is known there is one intersection point that fulfills Equation 4-6 for all satellites in view.

In the same matter as for the SD model the DD can be created, and again assuming short baselines ($\Delta^{pq}_{ij} \approx 0$) Equation 4-3 is rewritten as:

$$\Phi^{pq}_{ij} - \lambda N^{pq}_{ij} - \bar{\varepsilon}^{pq}_{\Phi,ij} = \|\mathbf{e}^{pq}_i\|\,\|\mathbf{b}\|\cos(\alpha^{pq}_{ij}) \tag{4-7}$$

Here $\mathbf{e}^{pq}_i$ is the line of sight vector of the virtual satellite s^{pq} at the position $\boldsymbol{\rho}^p_i - \boldsymbol{\rho}^q_i$. This vector should not be normalized ($\mathbf{e}^{pq}_i = \mathbf{e}^p_i - \mathbf{e}^q_i$) since the magnitude contains information

about the geometric representation. If the DD carrier phase measurements are used the number of equation will reduce with one as only $n_{sat} - 1$ virtual satellites can be created (the same satellite always needs to be taken as reference satellite s^p) from n_{sat} satellites in view. The rest of the section is described for the SD carrier phase measurements, although the BOUNDS algorithm uses the DD measurements. The difference being that one should consider virtual satellites in view and the receiver clock errors canceled out.

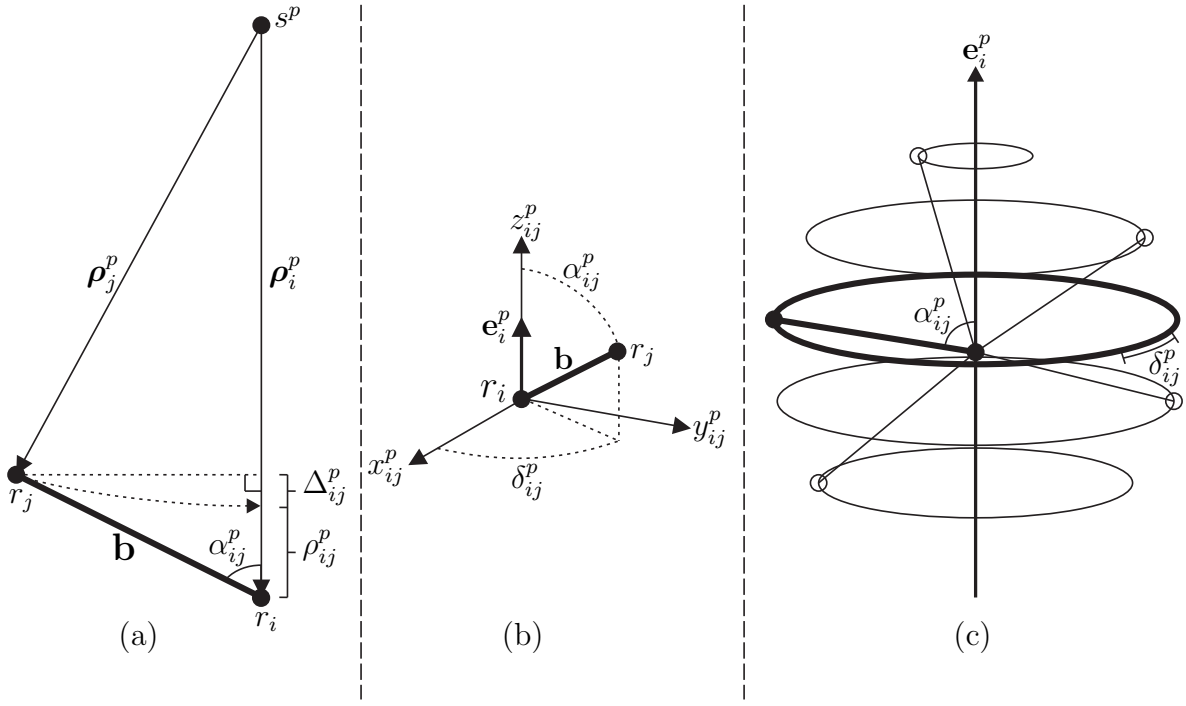

Figure 4-1: Geometric visualization of the SD integer ambiguity.

4-2-2 Possible Baseline Orientations

In this section it is assumed that the carrier phase measurements, baseline lengths and all other errors are correctly measured so the problem of finding the correct baseline orientation can be done with crisp numbers. This means finding the correct set of integers $\mathbf{N}_{ij} = \left(N_{ij}^1, ..., N_{ij}^{n_{sat}}\right)$ corresponding with the correct carrier phase measurements $\mathbf{\Phi}_{ij} = \left(\Phi_{ij}^1, ..., \Phi_{ij}^{n_{sat}}\right)$. This will start from Equation 4-6 where α_{ij}^p for each satellite is:

$$\alpha_{ij}^p = \cos^{-1}\left(\frac{\Phi_{ij}^p - \lambda N_{ij}^p - \bar{\varepsilon}_{\Phi,ij}^p}{\|\mathbf{e}_i^p\| \, \|\mathbf{b}\|}\right) \quad \text{for } p = 1, ..., n_{sat} \tag{4-8}$$

and the angle depends on the integer number. Feasible integer numbers are all that can create circles accordingly to Figure 4-1(c), that is:

$$-\left(\frac{\|\mathbf{e}_i^p\| \, \|\mathbf{b}\| + \Phi_{ij}^p + \bar{\varepsilon}_{\Phi,ij}^p}{\lambda}\right) \leq N_{ij}^p \leq \left(\frac{\|\mathbf{e}_i^p\| \, \|\mathbf{b}\| + \Phi_{ij}^p + \bar{\varepsilon}_{\Phi,ij}^p}{\lambda}\right) \quad \text{for } p = 1, ..., n_{sat} \tag{4-9}$$

The position of the baseline is described in spherical coordinates in the reference frame of Figure 4-1(b) and the position of r_j is:

$$\begin{bmatrix} x_j^p \\ y_j^p \\ z_j^p \end{bmatrix} = \|\mathbf{b}\| \begin{bmatrix} \sin\left(\alpha_{ij}^p\right)\cos\left(\delta_{ij}^p\right) \\ \sin\left(\alpha_{ij}^p\right)\sin\left(\delta_{ij}^p\right) \\ \cos\left(\alpha_{ij}^p\right) \end{bmatrix} \quad \text{for } \alpha_{ij}^p \in [-\pi, \pi],\ \delta_{ij}^p \in [0, 2\pi] \tag{4-10}$$

The angle δ_{ij}^p is dependent on the choice of x-axis direction, this is chosen to the cross product of $\mathbf{e}_i^p$ and $\mathbf{e}_i^q$ defined as:

$$x_{ij}^{pq} = \frac{\mathbf{e}_i^p}{\|\mathbf{e}_i^p\|} \times \frac{\mathbf{e}_i^q}{\|\mathbf{e}_i^q\|} \tag{4-11}$$

Further the angle δ_{ij}^p and reference frame F^p (Figure 4-1(b)) are rewritten as δ_{ij}^{pq} and F^{pq} respectively. Here the first superscripts denotes which satellite is used and the second which is used to compute the x-axis of the local reference frame. When intersecting two satellites, they need to be defined in the same reference frame. To do this the second satellite uses $\mathbf{e}_i^q$ as the local z-axis and the negative line of sight vector $-\mathbf{e}_i^p$ to compute the x-axis, this will ensure that the direction of both x-axis is the same. To compare the baseline orientation for both satellites a single rotation about the x-axis with the angle β_i^{pq} is required, defined as:

$$\beta_i^{pq} = \cos^{-1}\left(\frac{\mathbf{e}_i^p \cdot \mathbf{e}_i^q}{\|\mathbf{e}_i^p\|\,\|\mathbf{e}_i^q\|}\right) \tag{4-12}$$

All angles are visualized in Figure 4-2. The intersection of two satellite circles can be seen as the SD Equation 4-6, defined in the same reference frame. They should than yield the same position of the receiver r_j, that is:

$$\|\mathbf{b}\| \begin{bmatrix} \sin\left(\alpha_{ij}^q\right)\cos\left(\delta_{ij}^{q(-p)}\right) \\ \sin\left(\alpha_{ij}^q\right)\sin\left(\delta_{ij}^{q(-p)}\right) \\ \cos\left(\alpha_{ij}^q\right) \end{bmatrix} = \begin{bmatrix} 1 & 0 & 0 \\ 0 & \cos\left(\beta_i^{pq}\right) & \sin\left(\beta_i^{pq}\right) \\ 0 & -\sin\left(\beta_i^{pq}\right) & \cos\left(\beta_i^{pq}\right) \end{bmatrix} \|\mathbf{b}\| \begin{bmatrix} \sin\left(\alpha_{ij}^p\right)\cos\left(\delta_{ij}^{pq}\right) \\ \sin\left(\alpha_{ij}^p\right)\sin\left(\delta_{ij}^{pq}\right) \\ \cos\left(\alpha_{ij}^p\right) \end{bmatrix} \tag{4-13}$$

where superscript $(\bullet)^{q(-p)}$ stands for using $-\mathbf{e}_i^p$ to compute the x-axis. From the third row of Equation 4-13 the angle δ_{ij}^{pq} for which both circles intersect is obtained:

$$\delta_{ij}^{pq} = \sin^{-1}\left(\left(\frac{\cos\left(\alpha_{ij}^q\right) - \cos\left(\beta_i^{pq}\right)\cos\left(\alpha_{ij}^p\right)}{-\sin\left(\beta_i^{pq}\right)\sin\left(\alpha_{ij}^p\right)}\right) \cap [-1, 1]\right) \tag{4-14}$$

As the $\sin^{-1}$ function is only a mapping from $[-1, 1]$ to $[-\pi/2, \pi/2]$ there will be one more intersection points (or zero if $\delta_{ij}^{pq} = \emptyset$), the second at:

$$\delta_{ij}^{pq*} = sign(\delta_{ij}^{pq})\pi - \delta_{ij}^{pq} \tag{4-15}$$

The intersection points i and i^* are illustrated in Figure 4-2. The point where the circles for all satellites intersect is a valid baseline orientation for the integers $\mathbf{N}_{ij}$. To find this point all δ_{ij}^{pq} must be calculated for reference satellite s^p and the satellites in view s^q for

$q = 1, ..., n_{sat}\,,\ q \neq p$. As the angles will be defined in different coordinate frames F^{pq} they need to be transferred into one global reference frame F^{pQ}. As the z-axis is in the same direction for each reference frame the x-axis are also in the same plane. The transformation is a single rotation around the z-axis with the angle ω^{pqpQ} defined as:

$$\omega^{pqpQ} = \cos^{-1}\left(x_{ij}^{pQ} \cdot x_{ij}^{pq}\right) \tag{4-16}$$

This angle needs to be in the direction where the cross product of $x_{ij}^{pQ} \times x_{ij}^{pq}$ points in the direction of $\mathbf{e}_i^{pQ}$, if this is not true then the angle $\omega^{pqpQ} = 2\pi - \omega^{pqpQ}$ should be taken instead. The common intersection point for all circles is then:

$$\left[\alpha_{ij}^{pQ}, \delta_{ij}^{pQ}, \|\mathbf{b}\|\right] \quad \text{where} \quad \delta_{ij}^{pQ} = \bigcap_{q=1}^{n_{sat}} \left(\omega^{pqpQ} + \delta_{ij}^{pq}\right)\ ;\ q \neq p \tag{4-17}$$

If the intersection point is empty then the set of integers $\mathbf{N}_{ij}$ is not a correct solution for the baseline orientation.

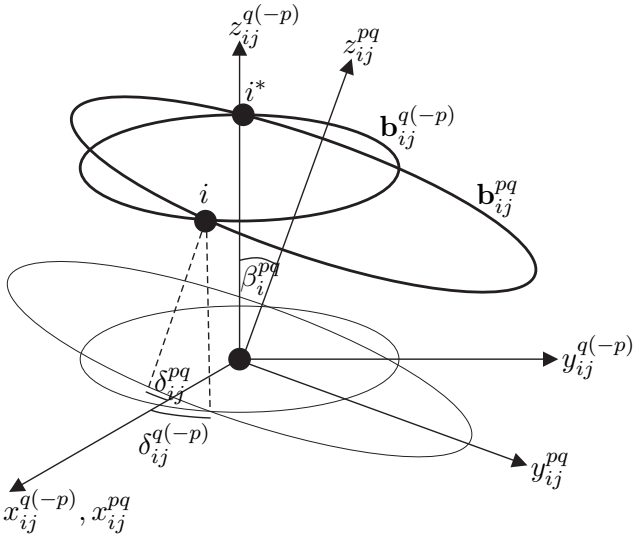

Figure 4-2: Angle and reference frame definitions of two intersecting circles.

4-2-3 Introducing Interval Analysis

Theoretically all the parameters in SD Equation 4-6 could be measured exactly in real life, though this is not possible, and thus the reason for introducing IA. Instead of working with crisp numbers intervals are introduced, to bound all error terms. The range of integers for satellite p is bounded by the interval $\left[N_{ij}^p\right]$ and the interval integer set vector is $[\mathbf{N}_{ij}] = \left(\left[N_{ij}^1\right], ..., \left[N_{ij}^{n_{sat}}\right]\right)$. The uncertainty of the baseline length is encapsulated by the interval base length $[\|\mathbf{b}\|]$. Further the carrier phase measurements and all other error terms are encapsulated by $\left[\Phi_{ij}^p\right] = \Phi_{ij}^p + \left[\bar{\varepsilon}_{\Phi,ij}^p\right]$ and the set vector of carrier phase measurements is $[\Phi_{ij}] = \left(\left[\Phi_{ij}^1\right], ..., \left[\Phi_{ij}^{n_{sat}}\right]\right)$. The cone angles α_{ij}^p will be transfered onto cone interval angles $\left[\alpha_{ij}^p\right]$ and Equation 4-8 is rewritten as:

$$\left[\alpha_{ij}^p\right] = \cos^{-1}\left(\frac{\left[\Phi_{ij}^p\right] - \lambda\left[N_{ij}^p\right]}{\|\mathbf{e}_i^p\|\,[\|\mathbf{b}\|]}\right) \tag{4-18}$$

The δ_{ij}^{pq} angle will be an interval angle $\left[\delta_{ij}^{pq}\right]$ and Equation 4-14 is rewritten as:

$$\left[\delta_{ij}^{pq}\right] = \sin^{-1}\left(\left(\frac{\cos\left(\left[\alpha_{ij}^{q}\right]\right) - \cos\left(\beta_{i}^{pq}\right)\cos\left(\left[\alpha_{ij}^{p}\right]\right)}{-\sin\left(\beta_{i}^{pq}\right)\sin\left(\left[\alpha_{ij}^{p}\right]\right)}\right) \cap [-1,1]\right) \tag{4-19}$$

The transformation to intervals is visualized in Figure 4-3. From Theorem 3-1-2 it can be guaranteed, that if the correct measurements are encapsulated by the intervals, Equation 4-18 to 4-19 will determine if the set $\mathbf{N}_{ij}, \mathbf{\Phi}_{ij}$ is a valid solution for the baseline orientation. This leads to an important theorem (van Kampen, 2010):

Theorem 4-2-3
If the following conditions are fulfilled:

$$\begin{aligned} \Phi_{ij}^{p} &\in \left[\Phi_{ij}^{p}\right] \quad for \quad p = 1, ..., n_{sat} \\ \|\mathbf{b}\| &\in [\|\mathbf{b}\|] \end{aligned} \tag{4-20}$$

and the intersection of all interval circles is an empty solution set:

$$\left[\delta_{ij}^{pQ}\right] = \emptyset \tag{4-21}$$

then the correct integer set is not in the current integer interval vector:

$$\mathbf{N}_{ij} = \left(N_{ij}^{1}, ..., N_{ij}^{n_{sat}}\right) \notin [\mathbf{N}_{ij}] = \left(\left[N_{ij}^{1}\right], ..., \left[N_{ij}^{n_{sat}}\right]\right) \tag{4-22}$$

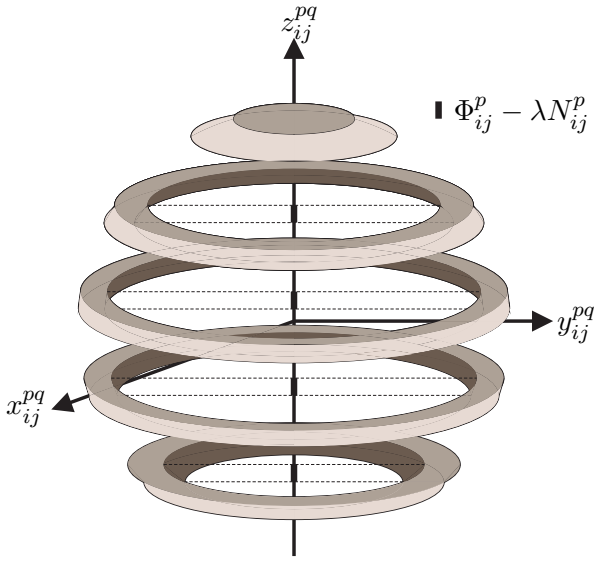

Figure 4-3: Visualization of the possible baseline orientation when introducing IA.

The above theorem will form a base for the BOUNDS algorithm where the incorrect integer set can be intervals. The rest of this section will introduce various methods to decrease the number of possible baseline orientations.

As was stated in Section 3-1-3 dependency will make the intervals wider, this is present in Equation 4-19 where the baseline length will occur multiple times as both $\left[\alpha_{ij}^{p}\right]$ and $\left[\alpha_{ij}^{q}\right]$ include the term. This is dealt with by the transformation from α angles to Z-intervals. This is illustrated as the thick bars in Figure 4-3 and defined as:

$$\left[Z_{ij}^{p}\right] = \left[\Phi_{ij}^{p}\right] - \lambda \left[N_{ij}^{p}\right] \tag{4-23}$$

The Z-intervals are inserted into Equation 4-18 to redefine $\cos\left(\left[\alpha_{ij}^{p}\right]\right)$ and $\sin\left(\left[\alpha_{ij}^{p}\right]\right)$ as:

$$\cos\left(\left[\alpha_{ij}^{p}\right]\right) = \frac{\left[Z_{ij}^{p}\right]}{\left[\|\mathbf{e}_{i}^{p}\|\right]\|\mathbf{b}\|} \tag{4-24}$$

$$\sin\left(\left[\alpha_{ij}^{p}\right]\right) = \sqrt{1 - \left(\frac{\left[Z_{ij}^{p}\right]}{\|\mathbf{e}_{i}^{p}\|\left[\|\mathbf{b}\|\right]}\right)^{2}} \tag{4-25}$$

Further if Equation 4-24 and 4-25 are inserted in Equation 4-19 it is reformulated as:

$$\left[\delta_{ij}^{pq}\right] = \sin^{-1}\left(\left(\frac{\left[Z_{ij}^{q}\right] - \cos\left(\beta_{i}^{pq}\right)\left[Z_{ij}^{p}\right]}{-\sin\left(\beta_{i}^{pq}\right)\sqrt{\left[\|\mathbf{b}\|\right]^{2} - \left[Z_{ij}^{p}\right]^{2}}}\right) \cap \left[-1,1\right]\right) \tag{4-26}$$

with only one occurrence of $[\|\mathbf{b}\|]$ and two of $\left[Z_{ij}^{p}\right]$. One other step that will be used later in the BOUNDS algorithm is the contractions, this allows to narrow the $\left[Z_{ij}^{q}\right]$ intervals. This is possible when the intersection interval $\left[\delta_{ij}^{pq}\right]$ is known, and from the third row of Equation 4-13 $\left[Z_{ij}^{q}\right]_{new}$ is defined as:

$$\left[Z_{ij}^{q}\right]_{new} = -\sin\left(\beta_{i}^{pq}\right)\sin\left(\left[\delta_{ij}^{pq}\right]\right)\sqrt{\left[\|\mathbf{b}\|\right]^{2} - \left[Z_{ij}^{p}\right]} + \left[Z_{ij}^{p}\right]\cos\left(\beta_{i}^{pq}\right) \tag{4-27}$$

The $\left[Z_{ij}^{q}\right]_{new}$ interval is subsequently intersected with the old $\left[Z_{ij}^{q}\right]$ interval to possible reduce the width.

Both the intersection and contraction equations have the dependency present due to the double occurrence of the variable $\left[Z_{ij}^{p}\right]$. This may lead to an overestimation of the intervals according to Section 3-1-3, which is solved using endpoint analysis. That is to check if the derivatives (with respect to $\left[Z_{ij}^{p}\right]$) of these functions are solely positive or negative for the entire interval, and if true use $\inf(\left[Z_{ij}^{p}\right])$ and $\sup(\left[Z_{ij}^{p}\right])$ in Equation 4-26 and 4-27. In Equation 4-26 the derivative is performed on $\sin\left(\left[\delta_{ij}^{pq}\right]\right)$ as the function $\sin^{-1}()$ does not ad

an extra $\left[Z_{ij}^{p}\right]$ term. The derivatives of Equation 4-26 and 4-27 are:

$$\frac{\partial \sin\left(\left[\delta_{ij}^{pq}\right]\right)}{\partial\left[Z_{ij}^{p}\right]} = \frac{\cos\left(\beta_{i}^{pq}\right)\left[\|\mathbf{b}\|\right]^{2} - \left[Z_{ij}^{p}\right]\left[Z_{ij}^{q}\right]}{\sin\left(\beta_{i}^{pq}\right)\left(\left[\|\mathbf{b}\|\right]^{2} - \left[Z_{ij}^{p}\right]^{2}\right)^{3/2}} \tag{4-28}$$

$$\frac{\partial\left[Z_{ij}^{q}\right]_{new}}{\partial\left[Z_{ij}^{p}\right]} = \frac{\sin\left(\beta_{i}^{pq}\right)\sin\left(\left[\delta_{ij}^{pq}\right]\right) + \cos\left(\beta_{i}^{pq}\right)\sqrt{\left(\frac{[\|\mathbf{b}\|]}{\left[Z_{ij}^{p}\right]}\right)^{2} - 1}}{\sqrt{\left(\frac{[\|\mathbf{b}\|]}{\left[Z_{ij}^{p}\right]}\right)^{2} - 1}} \tag{4-29}$$

The last part that may decrease the number of possible baseline orientations is the use of multiple frequencies. This is equivalent to adding an extra satellite when solving the problem but more efficient from the point of computational time. The Z-values for each frequency are expressed as $\left[Z_{ij}^{p}\right]_{f} = \left[\Phi_{ij}^{p}\right]_{f} + \lambda_{f}\left[N_{ij}^{p}\right]_{f}$ and as the baseline orientation is the same for each frequency these vectors are intersected for each satellite. The $\left[Z_{ij}^{p}\right]$ interval is then (n_{freq} is the number of frequencies):

$$\left[Z_{ij}^{p}\right] = \bigcap_{f=1}^{n_{freq}} \left[Z_{ij}^{p}\right]_{f} \tag{4-30}$$

When introducing IA we can guarantee that the correct integer numbers will be in the solution as stated by Theorem 4-2-3, but we can not guarantee that it will be the only solution. What happens when introducing IA is shown in Figure 4-4, that is, a second solution may occur (or many more depending on the width of the intervals of the carrier phase measurements and baseline length) due to more common intersection points. Here the intersections circles are only in one plane, for a more clear view.

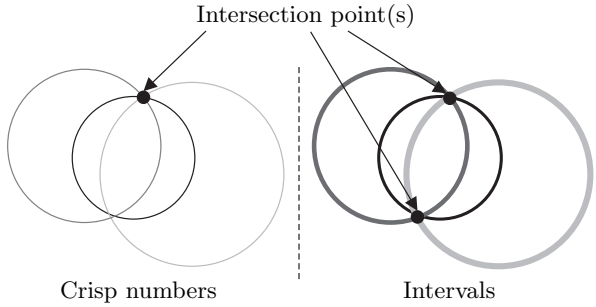

Figure 4-4: The effect on the number of intersection points when introducing IA.

4-2-4 Bounded Integer Ambiguity Resolution using Interval Analysis

The purpose is to find a solutions for the baseline orientation, expressed in $[\mathbf{Z}_{ij}]$ coordinates. This is done through the BOUNDS algorithm, that will start with the entire interval of integers and converges to possible baseline orientation. The algorithm can guarantee that if all errors are correctly bounded the correct solution will be found, although additional baseline orientation may appear (as seen in Figure 4-4). The schematic flowchart of the

BOUNDS algorithm is shown in Figure 4-6 and all the steps are described bellow.

The algorithm starts by defining the search space in coordinates of $[\mathbf{Z}_{ij}]_f$, this can be done for either one or two frequencies for the GPS, that is the L1 and L2 frequencies. At this point the noise bands of the carrier phase measurements need to be chosen. If there is no previous knowledge about the baseline orientation the search space should be chosen to lie in the interval $-\|[\|\mathbf{b}\|]\| \leq \left[Z_{ij}^q\right]_f \leq +\|[\|\mathbf{b}\|]\|$. Here satellite q is chosen in illustrations of the BOUNDS algorithm, but the same holds for all satellites. The first step is shown in Figure 4-5(a) where it is assumed that two frequencies are available.

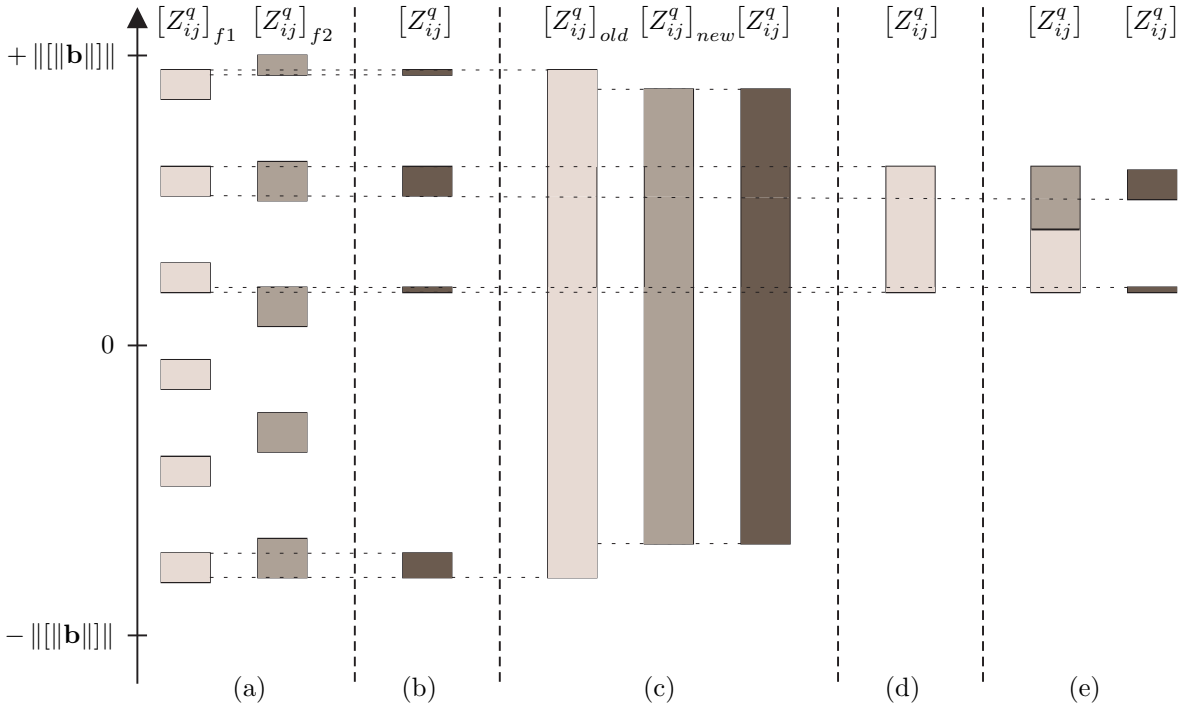

Figure 4-5: Illustration of how $\left[Z_{ij}^q\right]$ is contracted in the BOUNDS algorithm.

The second step of the algorithm intersects the two frequencies to obtain the interval $\left[Z_{ij}^q\right]$ which is illustrated in Figure 4-5(b). This step is only necessary if the number of frequencies is more than one. After this step the BOUNDS algorithm starts a loop, where the stopping criteria is to have all intervals in the matrix $[\mathbf{Z}_{ij}]$ (vector if only one solution) thin enough to only include one integer. In the third step the reference satellite p is chosen, for which the interval band is the smallest. The smallest interval band is defined as the sum of all intervals widths for satellite p.

In the fourth step the common intersection interval $\left[\delta_{ij}^{pq}\right]$ is calculated from Equation 4-26, this is done using endpoint analysis if Equation 4-28 is solely positive or negative. The $\left[\delta_{ij}^{pq}\right]$ values are transferred to the global reference frame F^{pQ} and the common intersection

interval is (can be an empty interval):

$$\left[\delta_{ij}^{pQ}\right] = \bigcap_{q=1}^{n_{sat}} \left(\omega^{pqpQ} + \left[\delta_{ij}^{pq}\right]\right) \; ; \; q \neq p \tag{4-31}$$

The fifth step is illustrated in Figure 4-5(c). The contracted $\left[Z_{ij}^{q}\right]_{new}$ is calculate from the common intersection interval, this is done using endpoint analysis if Equation 4-29 is solely positive or negative. The new Z-values are then intersected with $\left[Z_{ij}^{q}\right]_{old}$.

In the sixth step $\left[Z_{ij}^{q}\right]$ from Figure 4-5(c) is filtered with $\left[Z_{ij}^{q}\right]$ from Figure 4-5(b) to possible reduce the width (illustrated in Figure 4-5(d)). In the last step of the loop the $\left[Z_{ij}^{q}\right]$ values are bisected (only if the width is larger then the specified). The bisection is done through taking $m\left(\left[Z_{ij}^{q}\right]\right)$ and creating two intervals, these are filtered with $\left[Z_{ij}^{q}\right]$ from Figure 4-5(b) to possible reduce the width. This step is illustrated in Figure 4-5(e).

The algorithm will continue as long as all intervals are wider then the specified. Once all intervals are thin enough the $[\mathbf{Z}_{ij}]$ values for all possible baseline orientations are extracted. These values may be used to later calculate the relative position in different coordinate frames depending on the application. The transformation to aircraft attitude angles will be presented in Chapter 5.

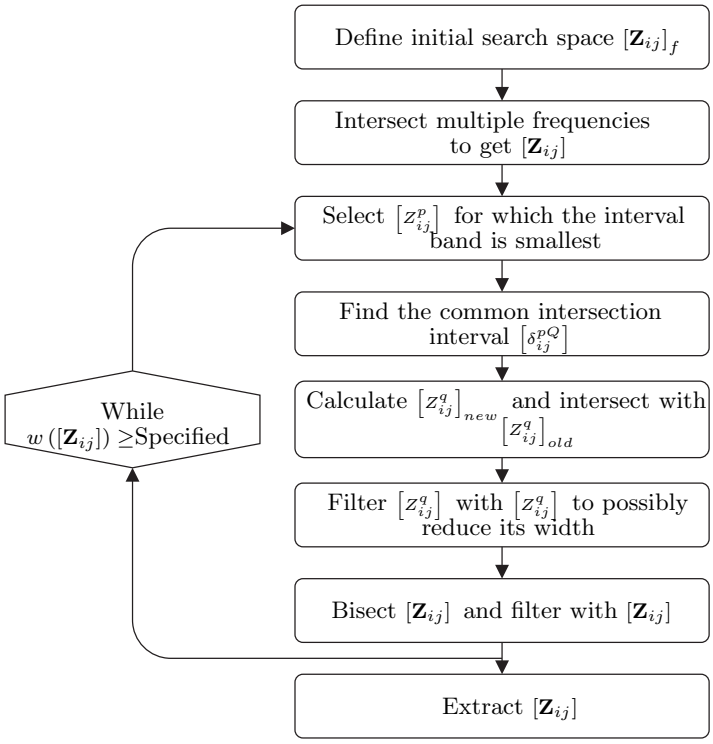

Figure 4-6: Schematic flowchart of the BOUNDS algorithm.

Chapter 5

Aircraft Attitude Determination

The spatial attitude of an aircraft is given by the three Euler angles, the pitch angle θ, the heading angle ψ and the bank angle φ. These are given with respect to the NED reference frame. The aircraft BF reference frame needs to be rotated in the correct order as the rotations are non-communicative, that is the angle ψ about the yaw axis, θ about the pitch axis and φ about the roll axis.

The current way to obtain these angles is with gyroscopes, but recent research has shown that the GPS carrier phase observations can be used to determine the Euler angles (van Kampen, 2010), (Buist, 2007). This chapter will give a short description of the gyros in the first section, and in the second section it will be explained in detail how relative positioning using multiple antennas is used to determine the Euler angles.

5-1 Attitude Determination with Gyroscopes

Most modern aircraft nowadays use gyroscopes to determine the attitude of the aircraft and there are two different systems, the stable platform and the strap down system. For the stable platform system the gyros are mounted on a platform which is suspended by four gimbals. This enables the system platform to move freely in all directions. The gimbals are then controlled by the gyros so that the platforms maintain in the same position regardless of the aircraft maneuvers. The position of the gimbals then provide a direct readout of the Euler angles. For the strap down system the the gyros are directly mounted onto a rigid part of the aircraft. The gyros will measure the angular rate of the aircraft, this rate is then integrated over time to obtain the angles with respect to an initial start angle. Nowadays most aircraft are mounted with the strap down system, as the accuracy is comparable to the stable platform system but they are more reliable and economical (Collinson, 2003).

The accuracy of the obtained attitude can vary with several orders of magnitude, as well as the price (Barbour & Schmidt, 2001). The accuracy can be measured by the rate

uncertainty of the gyros. For aircraft using gyros only for flight control systems the accuracy requirements are less than 1 deg/min. If a gyro is used as part of the inertial navigation system or fly by wire the rate uncertainty can not be larger than 0.01 deg/hour (Collinson, 2003). For flight control systems this means that in one minute the obtained angles can be up to one degree wrong, therefore these systems need to be rebooted often.

5-2 Attitude Determination Using Multiple Antennas

To determine the three Euler angles the relative position of the antennas is used. For attitude determination at least three antennas are necessary, and they can not be collinear. The attitude determination is divided into 5 steps:

1. Compute the baseline orientation in the form of $[\mathbf{Z}_{ij}]$.
2. Convert baseline orientation from $[\mathbf{Z}_{ij}]$ to Earth Centered Earth Fixed (ECEF) coordinates.
3. Convert baseline orientation from ECEF to NED coordinates.
4. Compute the Euler angles in antenna reference frame from the NED coordinates.
5. Transform the Euler angles in antenna reference frame to pitch, heading and bank angles.

The baseline orientation in $[\mathbf{Z}_{ij}]$ coordinates can be obtained using many different methods. For high precision attitude determination though, they need to be obtained from the carrier phase measurements. This can be done with one of the many methods presented in Chapter 4. In this section it is assumed that they are obtained from the BOUNDS algorithm.

Once these values are obtained they need to be converted first to ECEF coordinates. This is done from the line of sight vectors which are given in ECEF coordinates. The projection of the baseline interval vector $\left[\mathbf{b}^{ECEF}\right]$ in ECEF coordinates onto the line of sight vector is equal to the $[\mathbf{Z}_{ij}]$ coordinates, this can be expressed as following:

$$[\mathbf{Z}_{ij}] = \mathbf{e}\left[\mathbf{b}^{ECEF}\right] \tag{5-1}$$

And if the line of sight vectors for three satellites are known the baseline interval orientation in ECEF coordinates is:

$$\left[\mathbf{b}^{ECEF}\right] = \left(\mathbf{e}^T\mathbf{e}\right)^{-1}\mathbf{e}\,[\mathbf{Z}_{ij}] \tag{5-2}$$

The transformation from ECEF to NED coordinates is done when the position of one receiver is known. The accuracy of this position does not need to be high, and it can therefore be obtained from the PRN code observations. The baseline interval coordinates in NED are then (where the transformation matrix $\mathbf{T}^{ECEF\rightarrow NED}$ is given in Equation A-1):

$$\left[\mathbf{b}^{NED}\right] = \mathbf{T}^{ECEF\rightarrow NED}\left[\mathbf{b}^{ECEF}\right] \tag{5-3}$$

Before the fourth step is described the antenna and body reference system need to be defined, as well as the different baselines used for attitude determination. The antenna reference frame

$F^a = [X^a, Y^a, Z^a]$ and body reference frame $F^b = \left[X^b, Y^b, Z^b\right]$ are visualized in Figure 5-1, on the research airplane belonging to the NLR and DUT. The Euler attitude angles are always given with respect to F^b but this reference frame will not always be aligned with F^a. The Cessna Citation II airplane antenna reference frame is chosen so that the origin is in antenna one, at the fuselage of aircraft. The X^a-axis points from antenna 1 to antenna 2 at the nose of the fuselage. Further the direction of the Y^a-axis is chosen so that the all three antennas (the third being the one on the wingtip) lie in the X^aY^a-plane. The Z^a-axis is then chosen so to compile with the right hand notation of a reference frame. The three antennas will then form the baselines:

1. Fuselage-Nose from which the pitch and heading interval angles are calculated.

2. Fuselage-Wingtip from which the bank interval angle is calculated.

3. Wingtip-Nose.

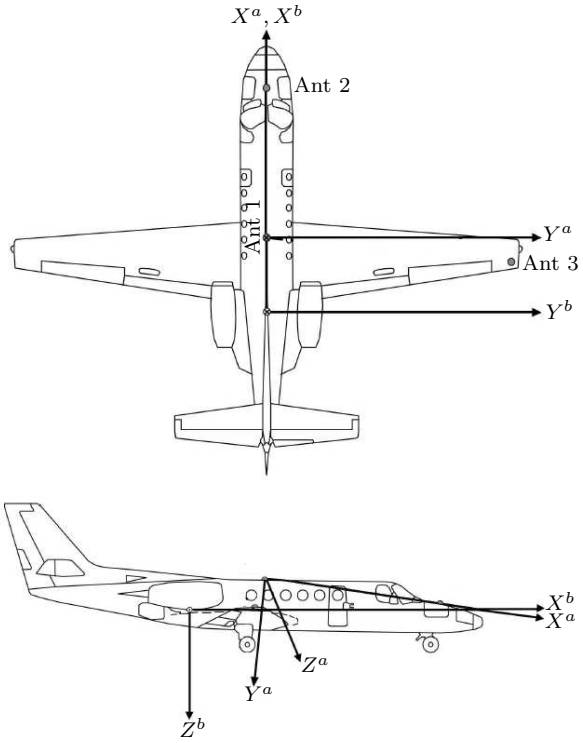

Figure 5-1: Antenna and body reference frames for Cessna Citation II research airplane.

In the fourth step the pitch and heading interval angles (in antenna reference frame) are calculated from the transformation of the baseline 1 (Fuselage-Nose) orientation coordinates in NED to antenna reference frame:

$$\left[\mathbf{b}_1^a\right] = \left[\mathbf{T}^{NED\rightarrow a}\right]\left[\mathbf{b}_1^{NED}\right] \tag{5-4}$$

where the interval transformation matrix $\left[\mathbf{T}^{NED\rightarrow a}\right]$ is given in Equation A-2 and $[\mathbf{b}_1^a] = [[\|\mathbf{b}\|], 0, 0]$. From Equation 5-4 the pitch and heading interval angles are:

$$[\theta^a] = \tan^{-1}\left(\frac{-\left[z_1^{NED}\right]}{\sqrt{\left[x_1^{NED}\right]^2 + \left[y_1^{NED}\right]^2}}\right) \tag{5-5}$$

$$[\psi^a] = \tan^{-1}\left(\frac{\left[y_1^{NED}\right]}{\left[x_1^{NED}\right]}\right) \tag{5-6}$$

where $\left[\left[x_1^{NED}\right], \left[y_1^{NED}\right], \left[z_1^{NED}\right]\right]$ are the interval coordinates of baseline 1 in the NED coordinate frame. To compute the bank interval angle the X-axis of the NED and antenna reference frame need to be aligned. This is done by first rotating baseline 2 (Fuselage-Wingtip) around the Z-axis of the NED reference frame with the interval heading angle, followed by a rotation around the Y-axis of the NED reference frame with the pitch interval angle. This is equivalent with rotating $[\mathbf{b}_2^a]$ around the X-axis of the antenna reference frame with the bank interval angle and expressed as:

$$R\left(-\left[\varphi^a\right]\right)\left[\mathbf{b}_2^a\right] = R\left(\left[\theta^a\right]\right)R\left(\left[\psi^a\right]\right)\left[\mathbf{b}_2^{NED}\right] \tag{5-7}$$

where the interval rotation matrices $R\left(\left[\theta^a\right]\right)$, $R\left(\left[\psi^a\right]\right)$ and $R\left(-\left[\varphi^a\right]\right)$ are given in Equation A-3 to A-5. From Equation 5-7 the bank interval angle is:

$$[\varphi^a] = \tan^{-1}\left(\frac{\left[z_1^{NED}\right]}{\left[y_1^{NED}\right]}\right) \tag{5-8}$$

After this the attitude angles in the BF reference frame are obtain by a final rotation that corrects for the offset of the antenna reference frame.

Part II

Implementation

Chapter 6

Experimental Setup

The BOUNDS algorithm is applied in off line simulations to investigate if it can be used for accurate attitude determination where only one (correct) solution remains. In the first section the setup of the simulation is explained, which is loosely based on the Cessna Citation II research airplane belonging to the NLR and DUT. Here the comparison of baseline orientation is explained in detail, as well as the GPS measurement simulator. In the second section the three investigations to be conducted are explained in detail.

6-1 Off line Setup

The simulations are based on the Cessna Citation II research airplane as there is earlier data to compare the off line simulations. The exact positions of the antennas are not known in the F^a reference frame, but only the length of the first two baselines in Figure 6-1, and from these the antenna coordinates are estimated. A fourth antenna is assumed to be mounted on the opposite wingtip. The coordinates of the antennas used during the simulations are given in Table 6-1. Figure 6-1 illustrates the six possible baselines when the Cessna Citation II research airplane is equipped with four antennas. In Table 6-1 the coordinates are given in the antenna reference frame and in the BF reference frame the antenna layout is symmetric. In Figure 6-1 b_1-b_6 are the different baselines that can be formed. With three receivers only three different baselines are obtained. When the extra antenna on the other wingtip is introduced three more baselines are obtained. Note that only two of the baselines are used for attitude determination, that is b_1 and b_2, the other ones are used in order to potentially reduce the number of solutions.

6-1-1 Comparing Baseline Orientations

The comparing of baselines orientation can reduce the number of possible airplane orientations (attitude angles) significantly. This is done by first calculating all baseline orientation in $[\mathbf{Z}_{ij}]$ intervals, these are transferred into ECEF interval coordinates using Equation 5-2.

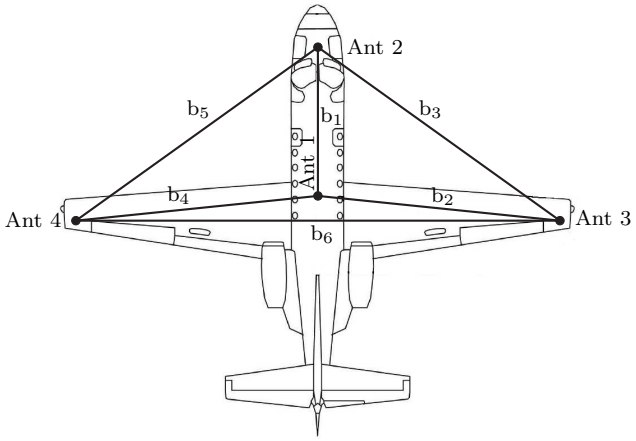

Figure 6-1: Visualization of the six possible baselines when the Cessna Citation II research airplane is equipped with four antennas.

Table 6-1: Coordinates of the Cessna Citation II research airplane antennas in the F^a reference frame, defined accordingly to Figure 5-1.

	X^a-coordinate [m]	Y^a-coordinate [m]	Z^a-coordinate [m]
Antenna 1	0	0	0
Antenna 2	5.456	0	0
Antenna 3	-1	7.5682	0
Antenna 4	-1	-7.2992	2

The $\left[\mathbf{b}^{ECEF}\right]$ relative baseline orientations can be seen as interval vectors, thus as illustrated in Figure 6-2(a) for the three antenna configuration, when adding the baseline 1 and 2 interval vectors it should yield in the orientation of the baseline three interval vector. If this is not true the combination of baseline interval vectors is not a valid solution for the airplane orientation. By trying all possible combinations for the baselines orientation interval vectors 1-3 accordingly to Figure 6-2(a) the number of airplane orientations can be reduced.

When adding an extra antenna the number of possible comparisons will be four, as illustrated in Figure 6-2(a)-(d). Thus the comparisons can be done four times to reduce the number of possible baseline orientations. For attitude determination only baselines 1 and 2 are necessary, the comparing can therefore stop when only one solutions is available for these. Further if all the comparisons in Figure 6-2 have been done, these can be repeated again as the number of possible baseline orientations may have decreased. A stopping criteria is when the number of solutions between two consecutive tests of comparing baselines for all combinations in Figure 6-2 are the same. In the BOUNDS algorithm the baselines are compared in the order from (a)-(d).

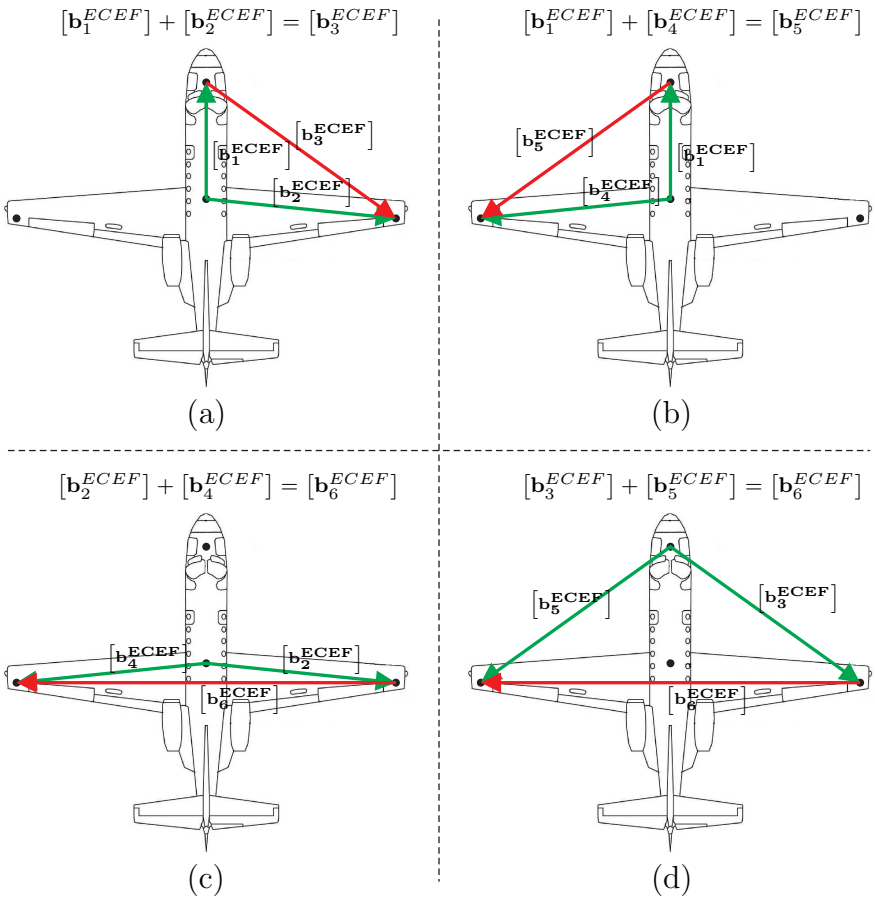

Figure 6-2: Possible baseline comparison configurations for the Cessna Citation II research airplane.

6-1-2 Measurement Simulator

The measurement simulator used for the thesis is developed by E. van Kampen for his PHD dissertation (van Kampen, 2010). This simulator is slightly modified to cope with three or four antennas. The simulator is loosely based on the GPS system, it consists of 24 satellites in six orbital planes (four in each plane) with an inclination of 55 degrees and semi major axis of 26600 km for all satellites . The position of each satellite is specified by its Kepler orbit elements and the satellites are equally distributed over each plane. The simulation starts by randomly choosing the Right Ascension of the Ascending Node (RAAN) offset angle between 0-60 degrees, with the same RAAN offset for each plane. Further the perigee for each plane is chosen randomly between 0-90 degrees. This means that all possible satellite configurations may occur.

The position of the satellites are then transferred to ECEF coordinates and the antenna positions are also given in ECEF coordinates. From this the line of sight vectors to each satellite are calculated, as well as the correct carrier phase measurements from each satellite to each receiver. These measurements are used to construct the correct SD carrier phase measurements and by subtracting two SD measurements from each other (with the same satellite as reference) the correct DD carrier phase measurements are obtained. A random error is added onto the measurements, this is uniformly distributed between the chosen noise limits. This will ensure that the correct carrier phase measurements are encapsulated by the noise bands. Thus when using the BOUNDS algorithm it is ensured that the correct baseline orientations are always found.

6-2 Experimental Configurations

The simulations are divided into three investigations. The first one investigates the effects of adding an extra antenna and frequency, in the second the noise levels on the L1 and L2 carrier phase measurements are varied and in the third investigation the noise levels on the baseline lengths are varied. For all investigation the baseline orientations are compared.

Further the simulations are done at two locations, Marcushof residence in the Netherlands ($N51°59'43.10"$, $E4°21'11.40"$) and AIK football arena ($N59°21'45.81"$, $E17°59'46.48"$) in Sweden at an altitude of 1000 meters. The Antenna 1 is always in the above given position and the attitude angles are randomly wandering. That is, initial pitch, heading and bank angles are chosen randomly, and then vary over time. The time steps are one second and each simulation consists of 500 epochs. Further it is assumed that there are no multipath effects, no restrictions on the pitch, heading and bank angle that the airplane can fly with, that the antennas always have a clear view of the satellites and that the cut off angle is zero degrees.

6-2-1 Introducing an Extra Frequency, Antenna and Comparing Baseline Orientations

Earlier results have just used one frequency in the BOUNDS algorithm as all antennas on the Cessna Citation II research airplane where not equipped with dual frequency receivers.

The simulations are therefore divided into three cases, in the first case only the L1 frequency is used, together with three antennas. In the second case one extra frequency is introduced and in the last step four antennas are used together with the two frequencies. For all cases the baseline orientations are compared in order to potentially reduce the number of solutions and all noise levels are kept constant.

For the L1 DD carrier phase measurements the noise diameter is 14 mm and for the L2 frequency 24.5 mm (van Kampen et al., 2009),(van Kampen, 2010). For the baseline lengths the noise radius for each baseline is given as a percentage of the total baseline length in Table 6-2, these values have been estimated roughly. The assumption is that antenna one is in a fixed position, further the flexibility of the airplane is denoted by the movement of the antennas 2-4. The second antenna is able to move ± 0.25 meters in the Z-direction of the BF reference frame and antennas three and four ± 0.5 meters. In Appendix B it is illustrated how the baseline 2 noise radius is estimated (all other are estimated in a similar way). The only varying parameter is the number of satellites in view, which is varied between 6-11. The range is chosen so that to prove that the two first cases will have more than one solution for the airplane orientation, even after CBO.

Table 6-2: Baseline length and noise radius estimations for the Cessna Citation II research airplane.

	$\mathbf{b_1}$	$\mathbf{b_2}$	$\mathbf{b_3}$	$\mathbf{b_4}$	$\mathbf{b_5}$	$\mathbf{b_6}$
Baseline length [m]	5.456	7.634	9.948	7.634	9.948	15.001
Baseline length noise radius [%]	0.5	1.5	0.25	1.5	0.25	0.25

6-2-2 Varying the Carrier Phase Noise Bands

This investigation is done only for the four antenna configuration with two frequencies. The number of satellites in view is eight, as most epochs from earlier results had eight satellites in view (Buist, 2007). The baseline noise radiuses are the ones estimated from Table 6-2 and kept constant for all simulations.

The varying parameter is the noise bands on the L1 and L2 carrier phase measurements. These are varied in a way that the ratio between the noise band of the L1 and L2 frequencies are kept constant at 1.75 (van Kampen et al., 2009). That is, the L2 noise band width is 1.75 times larger than that of L1. Further the L1 frequency is set to vary in between 14-40 mm for the DD carrier phase measurements (in steps of 2 mm). These simulations are done to see the effect on the number of solutions remaining when the noise bands are increased to simulate very noise receivers and antennas. The baseline orientations are compared in order to potentially reduce the number of solutions.

6-2-3 Varying the Baseline Length Noise Bands

In the last investigation the baseline length noise bands are varied. In the simulations the number of satellites in view is eight. Further the L1 and L2 carrier phase noise bandwidths are kept constant at 14 and 24.5 mm respectively. The baseline length noise radius is varied in between 0-4% in steps of 1% for all baselines b_1-b_6, that is in percentage of the nominal baseline lengths given in Table 6-2. The noise levels are chosen very high so to possibly see the effect on the number of solutions and simulate the unknown deflection (these have only been estimated earlier) of the airplane. The baseline orientations are compared in order to potentially reduce the number of solutions.

Chapter 7

Results

The chapter is divided into three section, each providing the main results to the investigation explained in Chapter 6, with the rest of the result presented in Appendix C. The main results are the percentage of epochs containing only one solution, the mean number of solutions, mean number of comparisons and mean computational times. These results are used to investigate if only one solution can be obtained for each epoch, with reasonably fast computational times and if the 4 antennas, 2 frequencies airplane configuration is necessary. Further the problems with overestimated intervals for the attitude angles are illustrated. It is important to notice that the noise (error) added onto the carrier phase measurements are not correlated. This as it is assumed that all satellite and receiver clock errors cancel out when using the DD carrier phase measurements and all other errors are uncorrelated. In reality there may be some correlation between the errors of the different receivers. For all simulations the correct attitude angles where found.

7-1 Introducing an Extra Frequency, Antenna and Comparing Baseline Orientations

Each simulation is 500 epochs, for each number of satellite in view. For the first case (3 antennas, 1 frequency) the simulations where only done at one location, the AIK football arena. For the two other cases the simulations where done at both the AIK football arena and Marcushof. This means that the first case has 3000 epochs in total, where as the second and third case have 6000 epochs each. The reason for the first case only being simulated once is that it is enough to show that the number of solutions will be more than one. Further the baseline noise levels for the first case are 10% of the ones presented in Table 6-2 as higher levels would yield to many solutions and computational overload. These noise levels are high enough to show that the 3 antennas, 1 frequency airplane configuration is not adequate to obtain only one solution for all epochs. The results from all simulations are tabulated in Tables C-1 to C-8.

In Figure 7-1 the percentage of epochs with only one solution is graphed versus the

number of satellites in view for all three cases, NCBO and CBO for baseline 1 and 2 as these are used to compute the pitch, heading and bank angles. The probability of obtaining one solution for NCBO is much higher for baseline 1 than baseline 2, which is due to the lower noise level on the baseline length. When the baseline orientations are compared though, the probability of obtaining one solution is almost equal for both baselines.

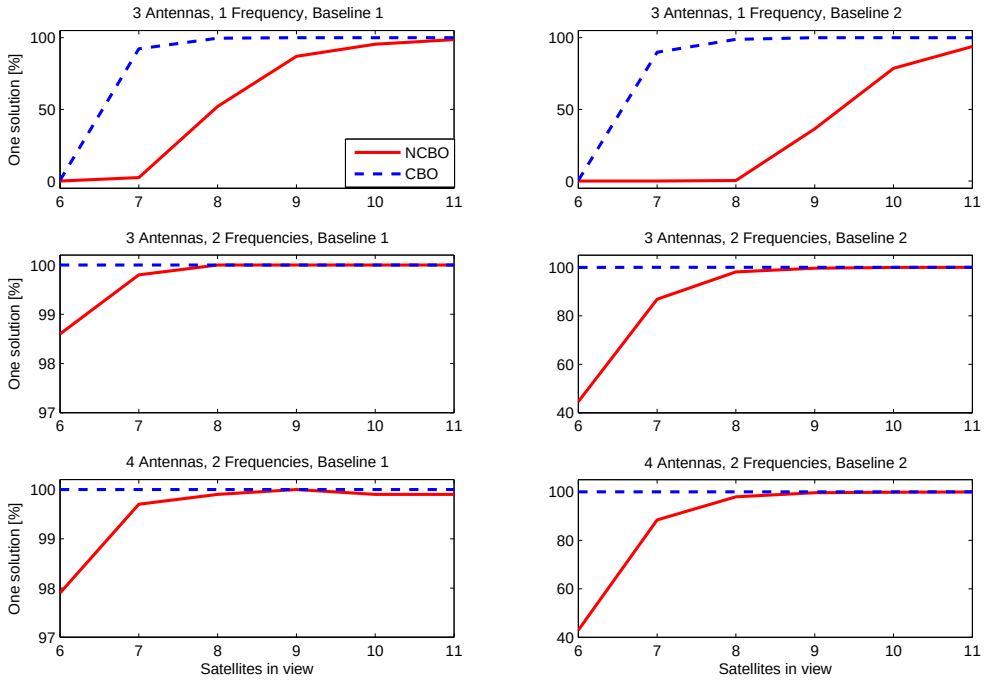

Figure 7-1: Percentage of epochs containing one solution for baseline 1 and 2, NCBO and CBO versus the number of satellites in view. Baseline length noise levels accordingly to Table 6-2 and the L1 and L2 carrier phase noise diameters 14 and 22.5 mm. For the 3 antennas, 1 frequency configuration the baseline length noise levels are 10% of the ones in Table 6-2.

Further from Table 7-1, if one solution is to remain for all epochs, the 3 antennas, 2 frequencies configuration is not adequate. Out of 1000 simulations with six satellites in view two solutions will remain for one of the epochs for baseline 2 after CBO.

In Figures 7-2 and 7-3 the effect of comparing the baselines orientations is illustrated. The bar diagrams show the distribution of remaining solutions for the 3000 epochs of the 3 antennas, 1 frequency configuration. The spread of the number of solutions is due to the fact that the number of satellites in view is varied between 6-11. From Figure 7-3 for baseline 2 the probability of obtaining one solution more than doubled for CBO. In Table 7-2 the min, max and mean number of solutions for the 3 cases are given, based on 3000 epochs (first case) and 6000 epochs (second and third case). When introducing a second frequency the average number of solutions for baseline 2, NCBO is around 65 times smaller. When the baseline orientations are compared for baseline 2, the average number of solutions is reduced by a factor of around 20 for the 3 antennas, 1 frequency airplane configuration. Further it

can be seen that the 4 antennas, 2 frequencies is the only configuration that can guarantee to always find only one solution (based on the 6000 epochs of simulations).

Table 7-1: Average percentage of epochs containing one solution for baseline 1 and 2, NCBO and CBO, for 6-11 satellites in view. Baseline length noise levels accordingly to Table 6-2 and the L1 and L2 carrier phase noise diameters 14 and 22.5 mm. For the 3 antennas, 1 frequency configuration the baseline length noise levels are 10% of the ones in Table 6-2.

	3 Antennas 1 Frequency	3 Antennas 2 Frequencies	4 Antennas 2 Frequencies
One Solution $\mathbf{b_1}$, NCBO [%]	55.90	99.73	99.55
One Solution $\mathbf{b_1}$, CBO [%]	82.07	100.00	100.00
One Solution $\mathbf{b_2}$, NCBO [%]	34.87	88.70	88.10
One Solution $\mathbf{b_2}$, CBO [%]	81.53	99.98	100.00

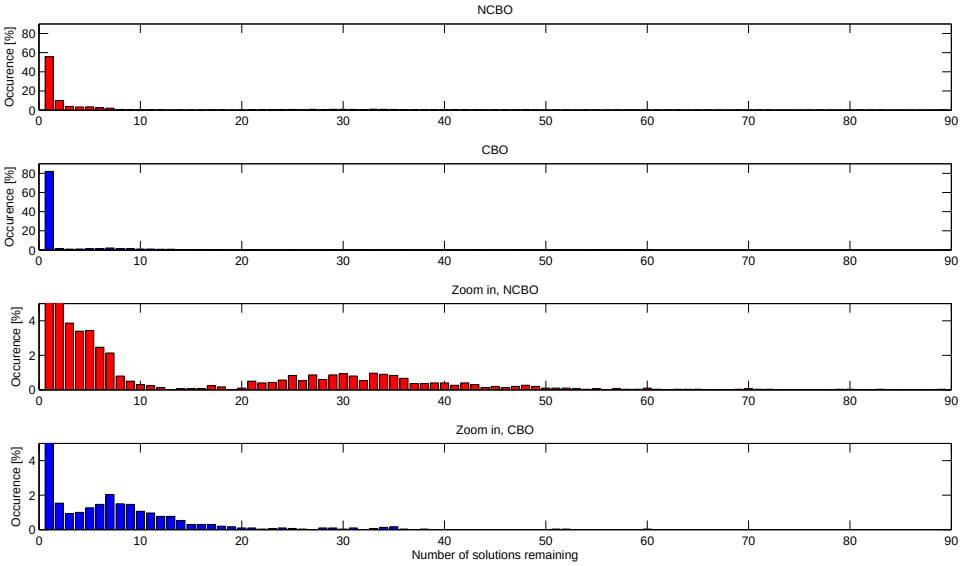

Figure 7-2: Distribution of remaining solutions baseline 1 for the 3 antennas, 1 frequency configuration, NCBO and CBO, based on 3000 epochs (6-11 satellites in view). The L1 carrier phase noise diameters is 14 mm and the baseline length noise levels are 10% of the ones in Table 6-2.

In Figure 7-4 the average computation time versus number of satellites in view is plotted for the 3 cases. The computation times are normalized with the minimal average computation time (3 antennas, 2 frequencies and seven satellites in view). As seen in Figure 7-4 the 3 antennas, 2 frequencies configuration has the fastest computational times. This is because the configuration obtains less solutions than the 3 antennas, 1 frequency configuration an does not have to calculate as many baseline orientations as the 4 antennas, 2 frequencies configuration. The fastest computational time for all the cases are with seven or eight

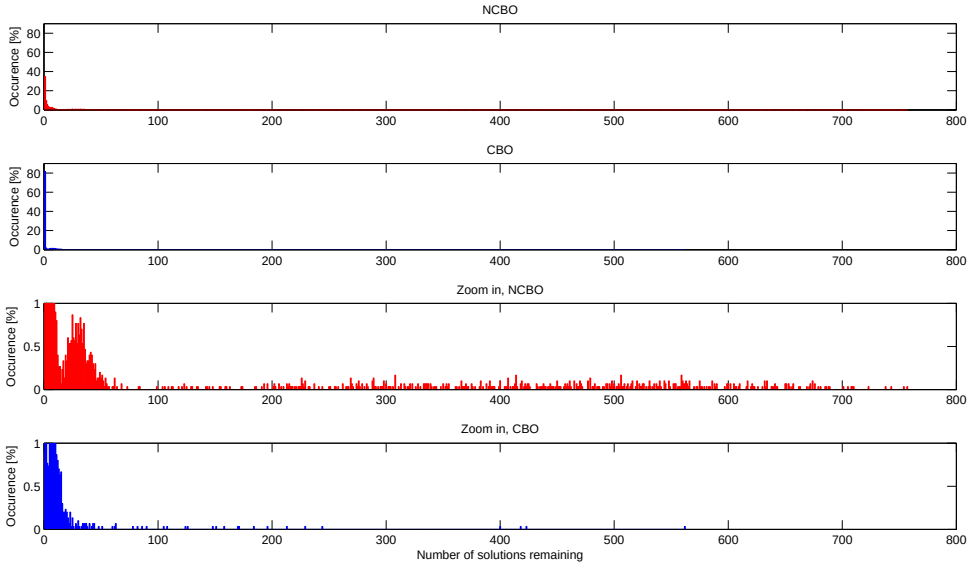

Figure 7-3: Distribution of remaining solutions baseline 2 for the 3 antennas, 1 frequency configuration, NCBO and CBO, based on 3000 epochs (6-11 satellites in view). The L1 carrier phase noise diameters is 14 mm and the baseline length noise levels are 10% of the ones in Table 6-2.

Table 7-2: Min, mean and max number of solutions remaining, NCBO and CBO, for 6-11 satellites in view. Baseline length noise levels accordingly to Table 6-2 and the L1 and L2 carrier phase noise diameters 14 and 22.5 mm. For the 3 antennas, 1 frequency configuration the baseline length noise levels are 10% of the ones in Table 6-2.

	$\mathbf{b_1}$, NCBO	$\mathbf{b_1}$, CBO	$\mathbf{b_2}$, NCBO	$\mathbf{b_2}$, CBO
3 Antennas, 1 Frequency				
Min	1	1	1	1
Mean	7.2867	2.5717	79.1093	4.2070
Max	89	60	757	562
3 Antennas, 2 Frequencies				
Min	1	1	1	1
Mean	1.0027	1.0000	1.1870	1.0002
Max	2	1	12	2
4 Antennas, 2 Frequencies				
Min	1	1	1	1
Mean	1.0047	1.0000	1.2007	1.0000
Max	3	1	10	1

satellites in view. The min, mean and max computational times are given in Table 7-3 for the three cases, based on 3000 epochs (first case) and 6000 epochs (second and third case). Table 7-3 is another example of why introducing one extra frequency is an advantage, as the computation times are significantly reduced. It also shows that the 3 antennas, 2 frequencies configuration can almost be used for real life applications as the sample time is one second and average computation time is 1.5 seconds. It should be noted the the BOUNDS algorithm has not been optimized for speed.

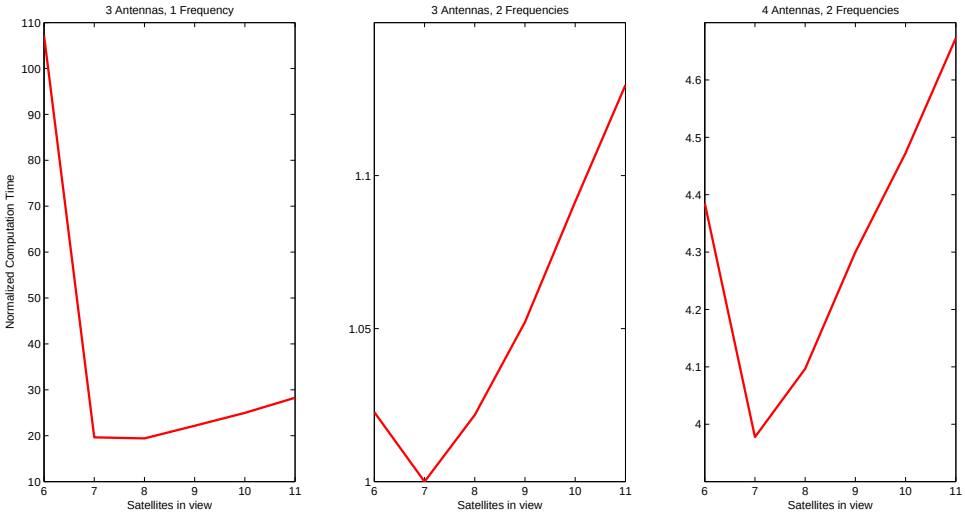

Figure 7-4: Average Computational times normalized with the min average computational time for the 3 antennas, 2 frequencies configuration versus number of satellites in view. Baseline length noise levels accordingly to Table 6-2 and the L1 and L2 carrier phase noise diameters 14 and 22.5 mm. For the 3 antennas, 1 frequency configuration the baseline length noise levels are 10% of the ones in Table 6-2.

Table 7-3: Min, mean and max computation times, 6-11 satellites in view. Baseline length noise levels accordingly to Table 6-2 and the L1 and L2 carrier phase noise diameters 14 and 22.5 mm. For the 3 antennas, 1 frequency configuration the baseline length noise levels are 10% of the ones in Table 6-2.

	3 Antennas 1 Frequency	3 Antennas 2 Frequencies	4 Antennas 2 Frequencies
Min [s]	19.08	0.97	2.52
Mean [s]	52.25	1.49	4.32
Max [s]	507.39	2.23	7.00

In Figures 7-5 to 7-7 the pitch, heading and bank angles are given for one of the simulations, together with the diameter of the solutions and Table 7-4 depicts the mean diameter and standard deviation. The Figures 7-5 to 7-7 illustrate the main issue when working with IA,

namely the overestimation of the intervals. This is mainly due to two steps in the IBIAR algorithm, the first being the transformation from Z-intervals to ECEF interval coordinate. The width of the obtained ECEF interval coordinates are dependent on the line of sight vectors used to transform the coordinates. The main issue of this is that it is not always possible to choose which line of sight vectors to use, and therefore control the width of the interval. This is due to that when many solutions are obtained one needs to choose the three satellites with the highest number of solutions (Z-intervals) so not to lose any baseline orientations. The second step that will only affect the width of the bank angle is that it is obtained through two extra rotations as explained in Chapter 5. These steps may therefor introduce an extra widening of the intervals. In Figures 7-5 to 7-7 the angles are in the antenna reference frame and in Figures C-1 and C-2 the worst case scenarios of attitude determination are illustrated. The min, mean and max diameters of the simulations for the 3 cases are given in Tables C-6 to C-8, from these values it is concluded that the accuracy of attitude determination are not very high for all epochs. In Chapter 9 recommendations on how to possible prevent this are given.

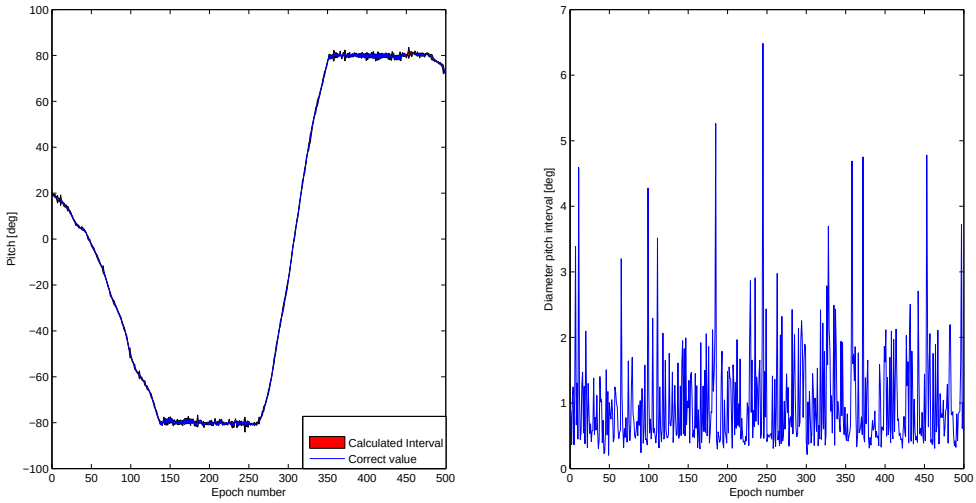

Figure 7-5: Simulated pitch angle, calculated pitch interval and diameter of the solution for an optimal case.

Table 7-4: Mean diameter and standard deviation of the obtained interval attitude angles in Figure 7-5 to 7-7.

	Mean Diameter [deg]	Standard Deviation [deg]
Figure 7-5	1.01	0.79
Figure 7-6	4.42	2.55
Figure 7-7	3.89	2.99

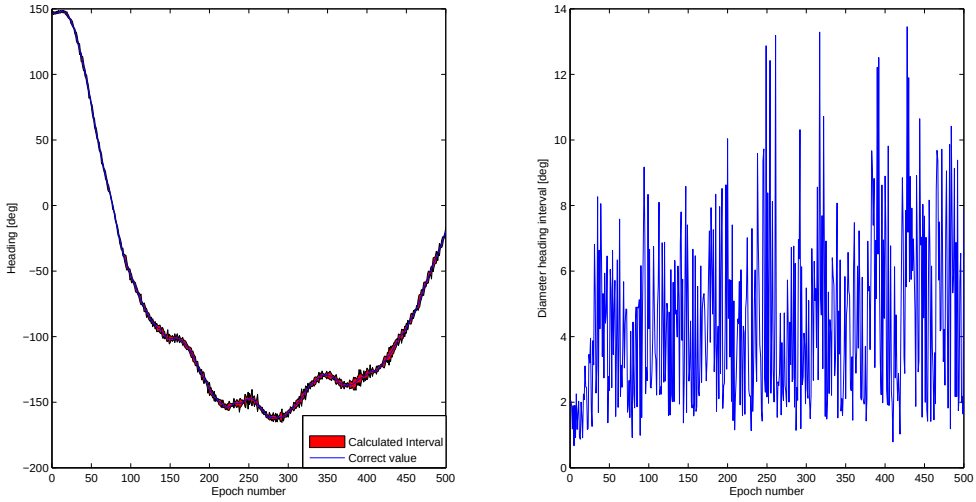

Figure 7-6: Simulated heading angle, calculated heading interval and diameter of the solution for an optimal case.

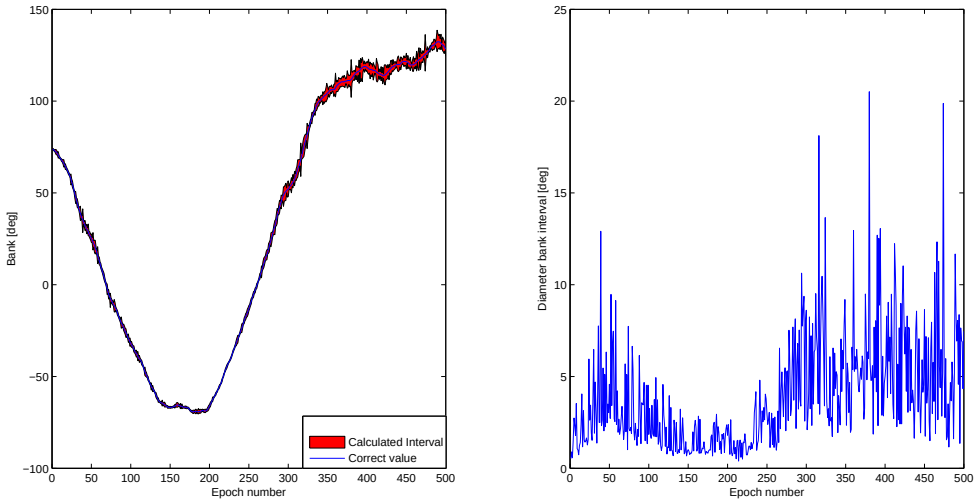

Figure 7-7: Simulated bank angle, calculated bank interval and diameter of the solution for an optimal case.

7-2 Varying the Carrier Phase Noise Bands

All simulations where performed at AIK football arena, with 500 epochs for each simulation, eight satellites in view and the baseline length noise radius according to Table 6-2 for the 4 antennas, 2 frequencies airplane configuration. The noise diameter of the L1 carrier phase measurements where varied from 14-40 mm in steps of 2 mm. That is equivalent to varying the noise radius from 3.67-10.5% of the carrier phase wavelength. The noise diameter of the L2 carrier phase measurements where varied from 24.5-70 mm keeping the ratio between the L1 and L2 noise diameter constant. That is equivalent to varying the noise radius from 5.01-14.31% of the carrier phase wavelength. No effect where seen on the accuracy of the obtained attitude angles and the main reason for that is explained in the previous section. The results from all simulations are tabulated in Tables C-9 to C-13.

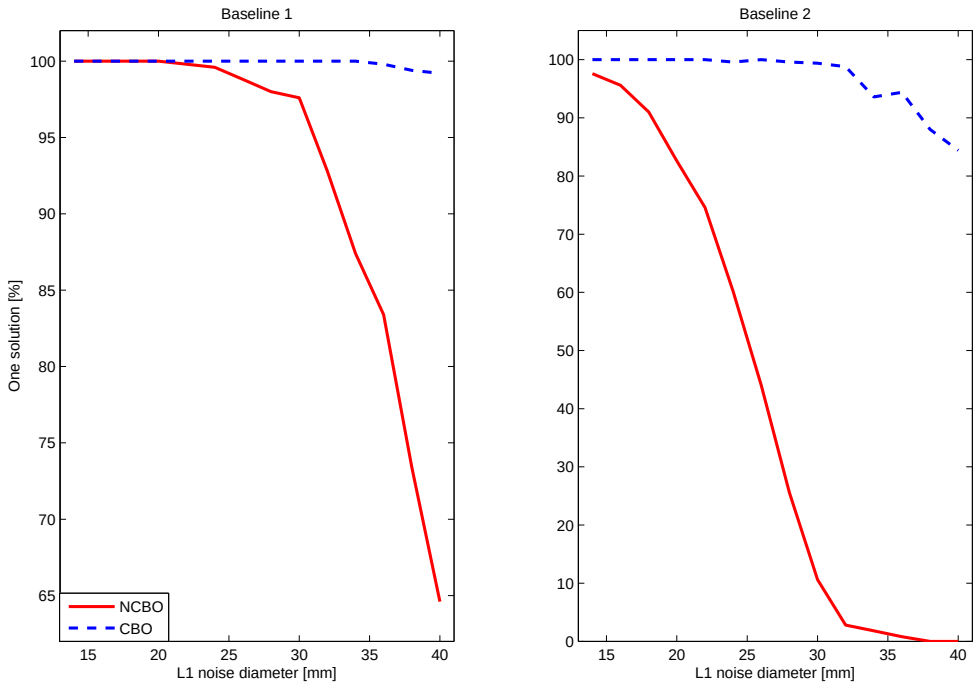

Figure 7-8: Percentage of epochs containing one solution for baseline 1 and 2 (4 antennas, 2 frequencies and eight satellites in view configuration), NCBO and CBO versus the noise diameter on the L1 carrier phase measurements. The noise diameter of the L2 carrier phase measurements are 1.75 times larger than the ones on the L1 frequency and the baseline length noise levels are given in Table 6-2.

In Figure 7-8 the percentage of epochs containing one solutions are plotted versus the noise diameter on the L1 carrier phase measurements, NCBO and CBO. The small peak in Figure 7-8 (baseline 2) for the 36 mm noise levels on the L1 carrier phase measurements is due to the low number of epochs used for each simulation. From Table C-9 it is concluded (based on the simulations made) that for up to 20 mm noise diameter on the L1 carrier phase measurements one solution is obtained for 100% of the epochs for baseline 1, NCBO.

For the baseline 2 one solution will never be obtained for all epochs of a simulation. When the baseline orientations are compared though, the noise levels are increased up to 36 mm (on the L1 carrier phase measurements) for baseline 1 before more than one solution occurs. For baseline 2 the noise diameter is increased up to 24 mm before more than one solution appears. Increasing the noise levels beyond these levels will rapidly decrease the percentage of epochs containing only one solution.

Figure 7-9 shows the average number of solutions remaining, NCBO and CBO for baseline 1 and 2. Before CBO it is seen that baseline 1 will have less solutions, but afterwards the number of solutions for both baselines will be almost equal. More importantly from Table C-11 it is conducted that for noise levels up to 30 mm on the L1 carrier phase measurements the number of solutions for baseline 2 will not be more than two. Increasing the noise levels further will rapidly increase the number of solutions, especially for baseline 2 which is used for bank angle determination.

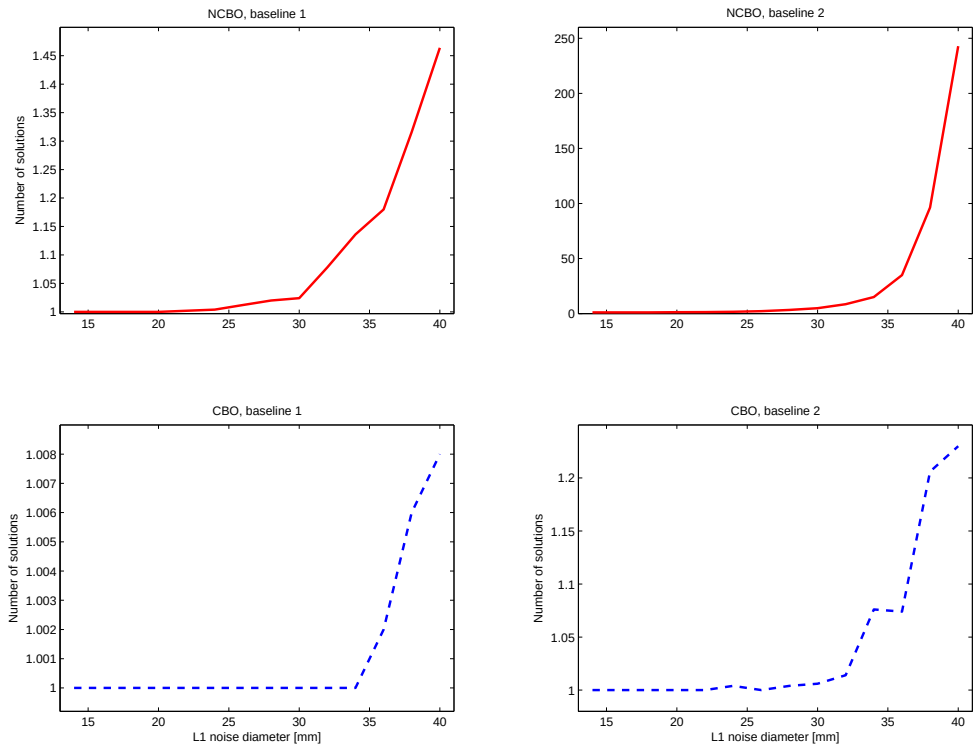

Figure 7-9: Average number of solutions remaining (4 antennas, 2 frequencies and eight satellites in view configuration), NCBO and CBO versus the noise diameter on the L1 carrier phase measurements. The noise diameter of the L2 carrier phase measurements are 1.75 times larger than the ones on the L1 frequency and the baseline length noise levels are given in Table 6-2.

In Figure 7-10 the normalized computational times and number of comparisons are graphed versus the noise levels on the L1 carrier phase measurements. These increase exponentially for both cases due to the exponential behavior of the number of solutions in Figure 7-9. The

dip in Figure 7-10 (Number of Comparisons) for the 36 mm noise levels on the L1 carrier phase measurements is due to the low number of epochs used for each simulation. The results in this section show that very high levels of noise can be added on the carrier phase measurements where only one solution remains (CBO). Further there is a certain break-point where the percentage of epochs containing one solution will decrease rapidly. It should be noted that the baseline 1, which always has much fewer solutions (before CBO) may be seen as a factor that allows the high noise levels on the carrier phase measurements. This leads to the last investigation, where it is assumed that all baseline lengths have the same percentage of noise levels.

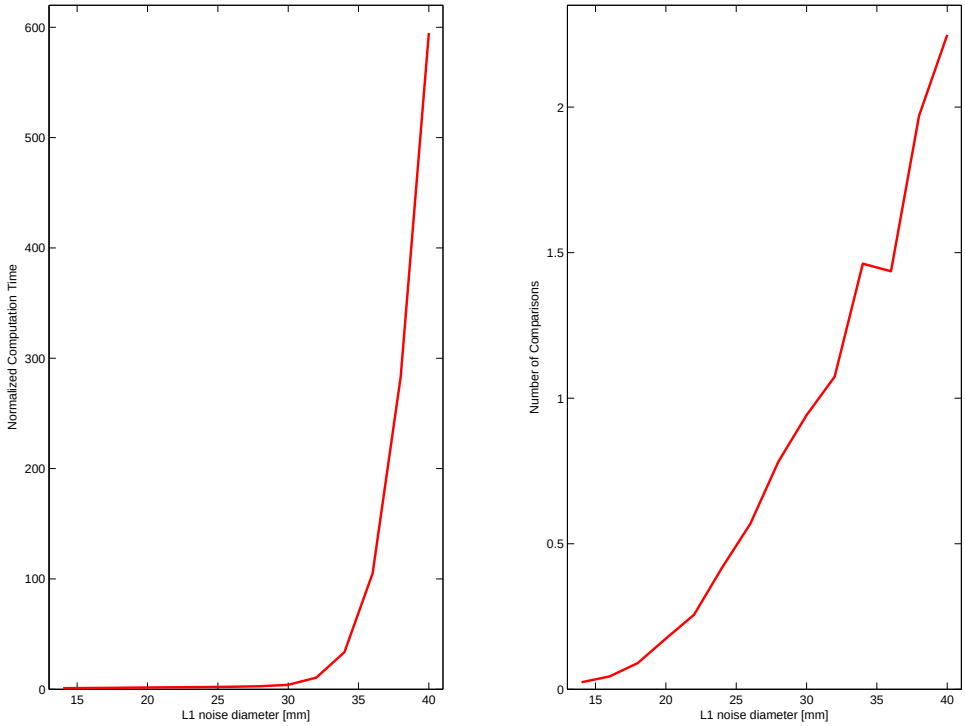

Figure 7-10: Average computation time normalized with the min average computational time and average number of comparisons (4 antennas, 2 frequencies and eight satellites in view configuration) versus the noise diameter on the L1 carrier phase measurements. The noise diameter of the L2 carrier phase measurements are 1.75 times larger than the ones on the L1 frequency and the baseline length noise levels are given in Table 6-2.

7-3 Varying the Baseline Length Noise Bands

All simulations where performed at AIK football arena, with 500 epochs for each simulation, eight satellites in view and the L1 and L2 carrier phase noise diameters 14 and 22.5 mm for the 4 antennas, 2 frequencies airplane configuration. The baseline length noise radius was varied from 0-4% in steps of 1%. No effect where seen on the accuracy of the obtained

attitude angles when increasing the noise. Further it should be noted that the noise levels on the baseline length are unrealisticly high for the Cessna Citation II research airplane. These levels where chosen so to possible see the effects on the number of solutions and percentage of epoch containing one solution, NCBO and CBO. No effect where seen on the accuracy of the obtained attitude angles and the main reason for that is explained in the previous section. The results from all simulations are tabulated in Tables C-14 to C-18.

In Figure 7-10 the percentage of epochs containing only one solution for baselines 1 and 2 are plotted versus the baseline length noise radius, NCBO and CBO. Baseline 1 will have more epochs containing only one solution for NCBO. This is because even though the baseline length radius is equal in percentage the baseline noise levels will be larger in length for the second baseline. The percentage of epochs containing one solution will decrease rapidly for both cases as the noise levels increase. When the baseline orientations are compared though, noise levels up to 4% will result in one solution for all cases (based on 500 epochs of simulations for each percentage).

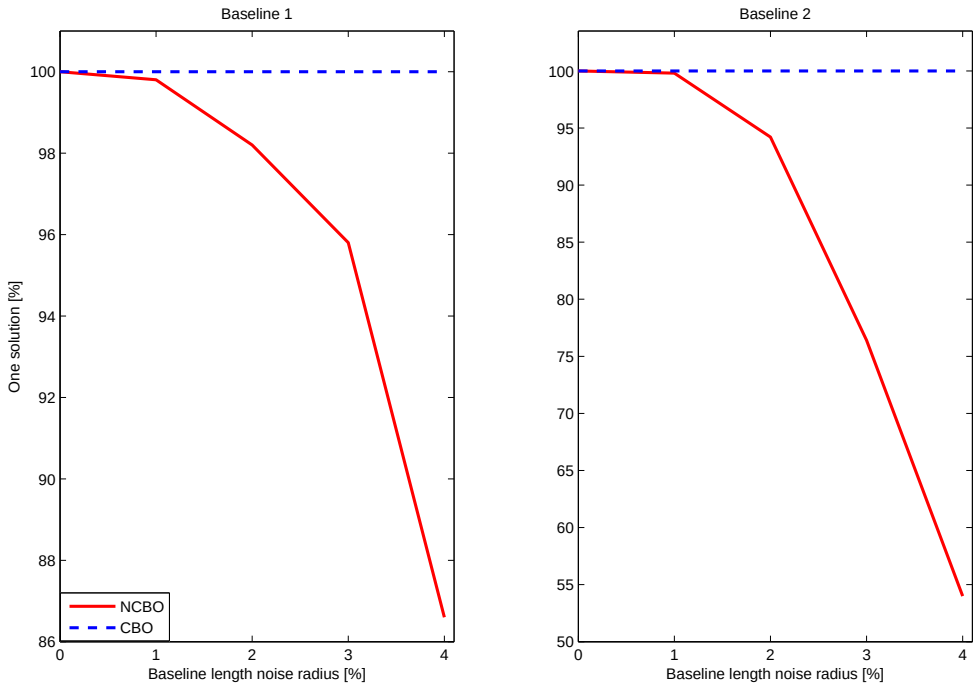

Figure 7-11: Percentage of epochs containing one solution for baseline 1 and 2 (4 antennas, 2 frequencies and eight satellites in view configuration), NCBO and CBO versus baseline length noise radius (equal percentage for all baselines). The L1 and L2 carrier phase noise diameters are 14 and 22.5 mm.

Figure 7-12 shows the average number of solution remaining, NCBO and CBO for baseline 1 and 2 versus the baseline length noise radius, from where it can be seen that for 0% baseline length noise radius one solution is always obtained for baseline 1 and 2 without comparing the baseline orientations. The average number of solutions for baseline 2 will further always

be larger than baseline 1 due to the higher noise levels in length.

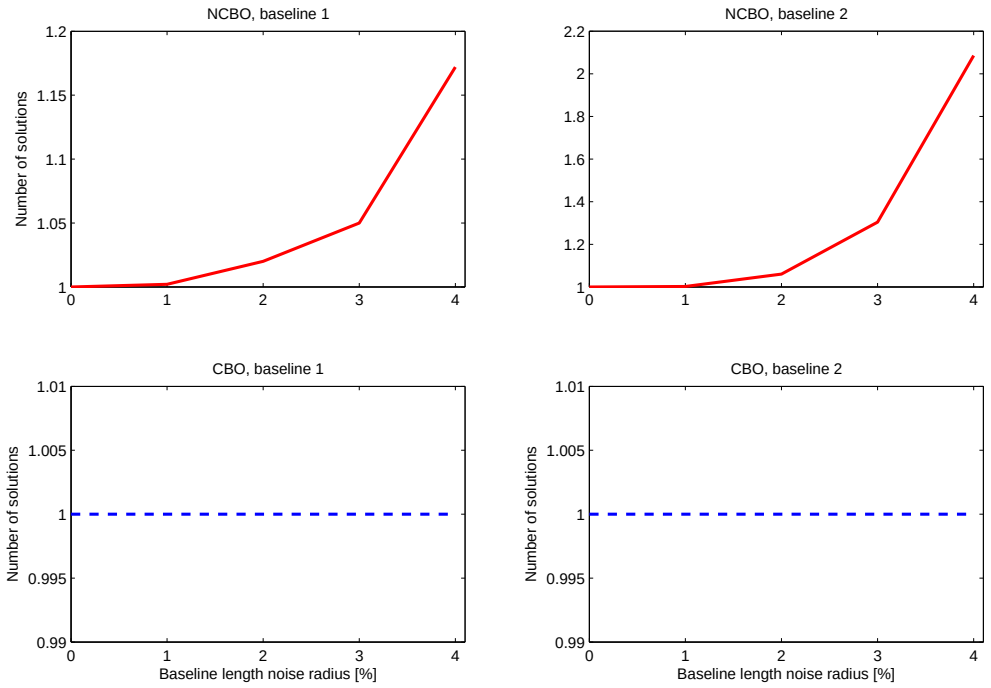

Figure 7-12: Average number of solutions remaining (4 antennas, 2 frequencies and eight satellites in view configuration), NCBO and CBO versus baseline length noise radius (equal percentage for all baselines). The L1 and L2 carrier phase noise diameters are 14 and 22.5 mm.

The main issues when increasing the baseline length noise radiuses are seen in Figure 7-13 where average computational time normalized with the min average computational time is graphed together with number of comparison. The computation times will increase dramatically after the baseline length noise radiuses are above 2%. The reason for this is the exponentially growing number of baseline configurations for baseline 6 and from Table C-17 it is seen that the computational times are well beyond real-time applications. Further it can be seen that the average number of comparisons is lower than one for all noise levels, and from Table C-18 maximum number of comparisons is not more than 3 for noise levels up to 4%. Thus the calculations of the baseline 6 orientation is not necessary for noise levels up to 4% (based on 500 epochs for each percentage).

It should be noted that the simulations were done for baseline noise radius up to 5%, though at these high levels the numbers of solutions (especially for baseline 6) increased dramatically. These simulations where not finished as too many solutions where found for one epoch and the computer froze.

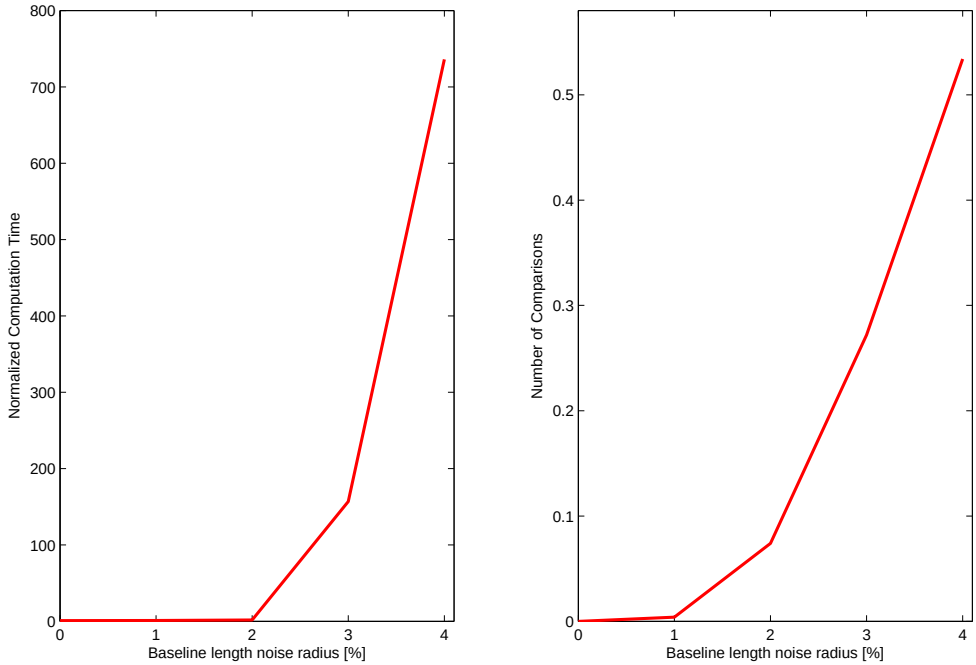

Figure 7-13: Average computation time normalized with the min average computation time and average number of comparisons (4 antennas, 2 frequencies and eight satellites in view configuration) versus baseline length noise radius (equal percentage for all baselines). The L1 and L2 carrier phase noise diameters are 14 and 22.5 mm.

Part III

Conclusions and Recommendations

Chapter 8

Conclusions

It should be noted that in the simulations there were no restrictions on the attitude angles and the antennas always had a clear view of the satellites above the cut off angle, this to put no restrictions on the initial search space. The geometry of the problem was loosely based on the Cessna Citation II research aircraft belonging to the NLR and DUT. Further the noise levels on the baseline lengths where only estimated. The objective of the thesis was to investigate if IBIAR could be used for accurate attitude determination where only one (correct) solution remains.

It can be concluded from the results that obtaining one solution is possible and the correct solution is always found as the correct measurements are always bounded by the noise bands. Obtaining a high accuracy (small diameter of the solutions) did not prove possible using the current BOUNDS algorithm though. How to improve this will be proposed in Chapter 9.

Further the BOUNDS algorithm in this thesis can not be used for real-time attitude determination as the average computational times are higher than the sample times. The BOUNDS algorithm was not optimized for speed and the computer used for the simulations was not optimized for the purpose of this thesis though. The conclusions from the three investigations are presented bellow.

Introducing an Extra Frequency, Antenna and Comparing Baseline Orientations
The comparing of the baseline orientations can reduce the number of solutions significantly for all three airplane configurations. This is most clearly viewed for the 3 antennas, 1 frequency configurations as the average number of solution reduces by a factor of 20 (baseline 2) when the baseline orientations are compared. From Table C-1 it can further be seen that if more than nine satellites are in view one solution will always be obtained for the 3 antenna, 1 frequency configuration (based on 500 epochs). It should be noted that this would imply much lower noise levels on the baseline lengths. It can therefore be concluded that the 3 antennas, 1 frequency configurations is not suitable if one solution is to remain (6-11

satellites in view), this has also been demonstrated by earlier data (van Kampen, 2010).

If one more frequency is added though, and the baseline length noise levels are much higher, only one out of 6000 epochs will contain more than one solutions. Further the computational times are rapidly decreased and this configuration could in many cases be seen as satisfactory. When a fourth antenna is introduced all the epochs will contain only one solutions, although computational times will increase as more baseline orientation need to be calculated. It can also be noted that it is not always necessary to use all the satellites in view (for the second and third case) as this may decrease the computational times. In real life applications this means that the cut off angle may be increased or some satellites that may introduce multipath effects may be neglected.

The results presented in Tables C-6 to C-8 and Figures C-1 to C-2 clearly indicate the problem of overestimated interval solutions. This due to the transformations from Z-intervals to ECEF interval coordinates. Noticeable though is that if the correct baseline solutions are obtained, that is the correct integers, and only one solution remains, the Z-coordinates may be transferred using crisp numbers. That is using the incorrect carrier phase measurements and the mid point of the baseline lengths when transferring from Z-coordinates to to attitude angles. The solution though, will not be the correct but the same as when using any of the other IAR techniques for attitude determination.

Varying the Carrier Phase Noise Bands
The main conclusions from the investigation of the carrier phase noise bands is that around 34 mm noise diameter (L1 frequency) there is a break point where the number of solutions will increase dramatically for baseline 2, NCBO. When the baseline orientations are compared though, the number of solutions for baseline 2 reduces significantly, this mainly as the other baselines have a lot less solutions. Also based on the simulations (500 epochs each noise level) for noise levels up to 22 millimeter the 3 antenna, 2 frequencies configuration is adequate as the max number of comparisons is one (Table C-13). This only valid for eight satellites in view.

Varying the Baseline Length Noise Bands
In the last investigation the effect of changing the baseline length noise radius were investigated. For these investigations the noise levels where overestimated to see any potential effects. It can be concluded that for any reasonable noise levels (up to 2%) which where tested, one solution was always obtained. Increasing the noise levels beyond these limits highly increased the computational time, which was due to that baseline 6 orientations had many solutions. For baseline length noise levels up to 4% though, baseline 6 was not used in comparing the baseline orientations and could have been disregarded. Based on the simulations (500 epochs each noise level) for noise levels up to 3% the 3 antennas, 2 frequencies configuration can be used as the max number of comparisons is one (Table C-18). This only valid for eight satellites in view.

One last point of interest are the angles measured when determining the attitude angles from the carrier phase measurements. It should be noted that these angles are the angles between two receivers of a flexible structure. These angles are not the same as the ones measured from gyroscopes, which are placed in a rigid part of the airplane and don't take care of the flexibility of the airplane. To determine these angles from the method presented

in the thesis there needs to be sensors that can measure the position of the antennas in the BF reference frame. Though the BOUNDS algorithm can be seen as measuring the true bank angle of the wing for example.

The end conclusion of the thesis is that the IBIAR method can be used for attitude determination where one (correct) solution remains but the accuracy of the solutions are very low. Chapter 9 gives recommendations on how to improve the accuracy of the attitude angles. On the base of the simulations done in the thesis the current BOUNDS algorithm should be applied to real data from the Cessna Citation II research airplane. It should be equipped with dual frequency receivers and although it is not necessary it is also recommended that it should be equipped with four antennas. For recommendations on future research see Chapter 9.

Chapter 9

Recommendations

The recommendations are divided into two parts, the first deals with recommendation on improvements of the BOUNDS algorithm. The second part gives recommendations on future research of the BOUNDS algorithm for attitude determination.

Improvements of the BOUNDS algorithm for attitude determination
The main issue of improvement is the diameter of the solutions, a problem clearly demonstrated in Figures C-1 and C-2. One way of dealing with the problem is to work with crisp numbers. This method will not find the correct attitude angles, but will give crisp solutions similar to the other IAR techniques presented in Section 4-1. This would work as following, the BOUNDS algorithm would first calculate and compare all the baseline orientations using IA, once these are known so are also all the correct integer combinations. Once the correct integers are known the attitude angles are obtained from the crisp measurements of the phase measurements and crisp baseline lengths (chosen to be the mid value). This technique may be improved if the error terms and baseline lengths are correctly estimated. Another way of improving this method is if the baseline length can be correctly measured with some means for each epoch, then the only unknown is the error of the carrier phase measurements. This error may be encapsulated by an interval band on the final attitude solutions. If this method is used and the baseline length is correctly measured the diameter of the pitch and heading angles will always be smaller than 0.65 degrees and for the bank angle the diameter will be smaller than 0.85 degrees. This is based on a noise diameter of 40 and 70 mm on the L1 and L2 carrier phase measurements respectively.

Another method that may reduce the diameter of the attitude angles is to try to use different reference satellites for the DD carrier phase measurements. Further if possible choose different combinations of virtual satellites when transforming from Z-intervals to ECEF interval coordinates. The choosing of virtual satellites for transformations may not be possible before the baseline orientations are compared, as one always needs to choose the three satellites with most Z-intervals. If after CBO for example only one attitude solution remains, this means that each virtual satellite only has one Z-interval. Choosing different virtual satellites for transformation from Z-intervals to ECEF interval coordinates may

therefore result in different diameters of the attitude angles. This method is an iterative process that may be used for post processing. From Tables C-6 to C-8 it can be seen that the min diameter of the solutions are very low, which can be seen as choosing the best combination of virtual satellites. This as each epoch uses three random virtual satellites when going from Z-intervals to ECEF interval coordinates.

For real-time applications the calculation speed of the BOUNDS algorithm needs to be improved. One of the ways to improve the speed is implementing it to work with other GNSS systems, especially the future GALILEO and COMPASS (assuming that the receiver are suitable). This may significantly improve the speed of the algorithm as much more frequencies are available, this is a way of reducing the possible Z-intervals in the beginning of the algorithm in a very fast mater.

Further the BOUNDS algorithm does not always have to compute all the baseline orientations, as illustrated in Section 7-3 where the baseline six was never used but took most of the computational time to find the correct baseline orientations. This could be solved by calculating the baseline orientation of each baseline separately, and compare the baseline orientations as soon as it is possible. This would allow the BOUNDS algorithm to stop before all the possible orientations of baseline six are calculated and reduce the computational time.

Other ways of reducing the computational speed is to not always use all the satellites in view, as seen in Figure 7-4 where the min average computational time is for 7-8 satellites in view. If the noise levels are low this is enough satellites to find one solution. Further this may also be used to potentially avoiding multipath effect by not using the satellites in view that may be subject to this effect.

A last way of reducing the computational speed (and also the number of possible baseline orientations) is reducing the initial search space. For most applications the pitch and bank angles of the aircraft are bounded to lie within small intervals (as for the Cessna Citation II research airplane), these may be directly transferred to reducing the initial Z-interval search space.

Future research
The main research that needs to be conducted is that on real flight data from the Cessna Citation II research aircraft. For this to be possible though, it would be needed that the airplane was equipped with four dual frequency receivers. This would make it possible to conduct all the simulations presented in Chapter 7. Although it would also be favorable to equip the airplane with some sort of device to accurately measure the distance between all the receivers for all epochs. This would make it possible to both check if it in reality is possible to obtain one solution for all cases and to conduct work on reducing the width of the solutions using the different methods presented above. This could first be developed as post processing tool for attitude determination and then later hopefully as a real-time attitude determination system.

For a more clear view of the noise limits on baseline lengths and carrier phase measurements the simulations in Subsections 6-2-2 and 6-2-3 should be conducted for 6-11 satellites in view, this could also be done with real flight data if available. Further it

should be investigated (preferable prior to installing new antennas on the Cessna Citation II research aircraft) the effect of where the antennas are positioned, on both the accuracy, number of solutions and multipath effect. The effect of not encapsulating the correct carrier phase measurement and baseline lengths by the noise bands should be investigated, as for real flight data this may happen.

A last investigation should also be made into the correlation between the errors for different receivers, and their effect on the number of solutions and diameters of the solutions. This has not been made in the thesis or any previous work on the IBIAR ((de Weerdt et al., 2008), (van Kampen et al., 2009) and (van Kampen, 2010)).

An investigation that has not yet been conducted is one with long baselines. A length that could be considered interesting is the one where the ionospheric and tropospheric delays would cancel out but the correction term for long baselines would not be zero. This is baseline lengths up to a few kilometers. This could be seen as having one or more receivers on the ground and forming the baselines between the ground antennas and airplane antennas. If these baseline orientations are calculated both the attitude of the airplane and and the precise position of the airplane would be known. For this to be possible though, the initial search space would have to be bounded (we know the approximate position of the airplane) otherwise the search would be extremely large (long computational times). This application could be especially interesting for aircraft landing systems and UAV, so to precisely know both the attitude and position of the aircraft.

Bibliography

Barbour, N., & Schmidt, G. (2001). Inertial Sensor Technology Trends. *IEEE Sensors Journal*, *1*(4), 332-339.

Buist, P. (2007). The Baseline Constrained LAMBDA Method for Single Epoch, Single Frequency Attitude Determination Applications. In *ION GNSS 20th Internationa Technical Meeting of the Satellite Division* (p. 2962-2973). Fort Worth, TX, USA.

Collinson, R. P. G. (2003). *Introduction to Avionics Systems* (2nd ed.). Kluwer Academic Publishers.

Computer Science Bibliography. (2011). *References to papers on Interval.* `http://liinwww.ira.uka.de/bibliography/?query=interval&case=off&partial=on`.

de Weerdt, E., van Kampen, E., Chu, Q. P., & Mulder, J. A. (2008). New Approach for Integer Ambiguity Resolution using Interval Analysis. *NAVIGATION, Journal of The Institute of Navigation*, *55*(4), 293-307.

Eldredge, L. (2011). *WAAS and LAAS Program Status.* `www.navcen.uscg.gov/pdf/cgsicMeetings/50/[27]Eldredge_*WAAS_*LAAS.pdf`.

European Space Agency. (2011). *Information about GALILEO.* `www.esa.int/esaNA/index.html`.

Han, S., & Rizos, C. (1996). Improving the computational efficiency of the ambiguity function algorithm. *Journal of Geodesy*, *70*(6), 330-341.

Hofmann-Wellenhof, B., Lichtenegger, H., & Collins, J. (2001). *GPS Theory and Practise* (5th ed.). Springer-Verlag Wien New York.

Inside GNSS. (2011). *Information about COMPASS.* `www.insidegnss.com/compass`.

Jaulin, L., Kieffer, M., Didrit, O., & Walter, E. (2001). *Applied Interval Analysis.* Springer-Verlag London Berlin Heidelberg.

Kaplan, E. D., & Hegarty, C. J. (2006). *Understanding GPS Principles and Applications* (2nd ed.). ARTECH HOUSE, INC.

Kim, D., & Langley, R. B. (2000). GPS Ambiguity Resolution and Validation: Trends and Issues. In *7th GNSS Workshop - International Symposium on GPS/GNSS.* Seoul, Korea.

Lorga, J. F. M. (2006). *Precise Navigation Using GPS.* Master thesis, Faculty of Aerospace Engineering, Delft University of Technology.

Misra, P., & Enge, P. (2006). *Global Positioning System: Signals, Measurements, and Performance* (2nd ed.). Ganga-Jamuna Press.

Moore, R. E., Baker Kearfoot, R., & Cloud, M. J. (1966). *Introduction to Interval Analysis.* Prentice-Hall Inc.

Notice Advisory to NAVSTAR Users. (2011). *GPS constellation status.* `www.navcen.uscg.gov/?pageName=GPS`.

Rump, S. M. (2011). *INTerval LABoratory.* `www.ti3.tu-harburg.de/~rump/intlab/`.

Teunissen, P. J. G. (1995). The least-squares ambiguity decorrelation adjustment: a method for fast GPS integer ambiguity estimation. *Journal of Geodesy*, *70*, 65-82.

Teunissen, P. J. G. (1999). An optimality property of the integer least-squares estimator. *Journal of Geodesy*, *73*, 587-593.

van Kampen, E. (2010). *Global Optimization using Interval Analysis: Interval Optimization for Aerospace Applications.* PhD thesis, Faculty of Aerospace Engineering, Delft University of Technology.

van Kampen, E., de Weerdt, E., Chu, Q. P., & Mulder, J. A. (2009). Applied Interval Based Integer Ambiguity Resolution. *NAVIGATION, Journal of The Institute of Navigation*, *56*(3), 205-219.

Ventura-Traveset, J., Gauthier, L., Toran, F., de Lesthievent, C., & Bedu, J. Y. (2005). EGNOS Status, performance and Planned Evolutions (2006-2010). In *Egnos Navigation Conference.* Munich, Germany.

Part IV

Appendices

Appendix A

Reference Frame Transformations and Rotations Matrices

This appendices states all the transformation and rotation matrices used in the thesis where most of the information is taken from (Lorga, 2006). In all equation $\sin()$ and $\cos()$ are represented by $s()$ and $c()$ and in Equation A-2 to A-5 the interval notation is drooped.

The transformation matrix from F^{ECEF} to F^{NED} is:

$$\mathbf{T}^{ECEF\rightarrow NED} = \begin{bmatrix} -c(\varphi_{glat})\,c(\lambda_{long}) & -c(\varphi_{glat})\,s(\lambda_{long}) & s(\varphi_{glat}) \\ -s(\lambda_{long}) & c(\lambda_{long}) & 0 \\ -s(\varphi_{glat})\,c(\lambda_{long}) & -s(\varphi_{glat})\,s(\lambda_{long}) & -c(\varphi_{glat}) \end{bmatrix} \tag{A-1}$$

where λ_{long} is the longitude and φ_{glat} is the geocentrical latitude of the airplane. The transformation matrix from F^{NED} to F^{a} is:

$$\mathbf{T}^{NED\rightarrow a} = \begin{bmatrix} c(\theta^a)\,c(\psi^a) & s(\varphi^a)\,s(\theta^a)\,c(\psi^a) - c(\varphi^a)\,s(\psi^a) & c(\varphi^a)\,s(\theta^a)\,c(\psi^a) - s(\varphi^a)\,s(\psi^a) \\ c(\theta^a)\,s(\psi^a) & s(\varphi^a)\,s(\theta^a)\,s(\psi^a) - c(\varphi^a)\,c(\psi^a) & c(\varphi^a)\,s(\theta^a)\,s(\psi^a) - s(\varphi^a)\,c(\psi^a) \\ -s(\theta^a) & s(\varphi^a)\,c(\theta^a) & c(\varphi^a)\,c(\theta^a) \end{bmatrix} \tag{A-2}$$

The rotation matrices are:

$$R(\theta^a) = \begin{bmatrix} c(\theta^a) & 0 & -s(\theta^a) \\ 0 & 1 & 0 \\ s(\theta^a) & 0 & c(\theta^a) \end{bmatrix} \tag{A-3}$$

$$R(\psi^a) = \begin{bmatrix} c(\psi^a) & s(\psi^a) & 0 \\ -s(\psi^a) & c(\psi^a) & 0 \\ 0 & 0 & 1 \end{bmatrix} \tag{A-4}$$

$$R(-\varphi^a) = \begin{bmatrix} 1 & 0 & 0 \\ 0 & c(\varphi^a) & -s(\varphi^a) \\ 0 & s(\varphi^a) & c(\varphi^a) \end{bmatrix} \tag{A-5}$$

Appendix B

Baseline Noise Radius Estimations

The baseline noise levels are only estimations. The calculations of baseline noise levels are only illustrated for baseline 2 (and baseline 4 due to symmetric antenna layout) and Figure B-1 shows how the baseline 2 noise radius is estimated.

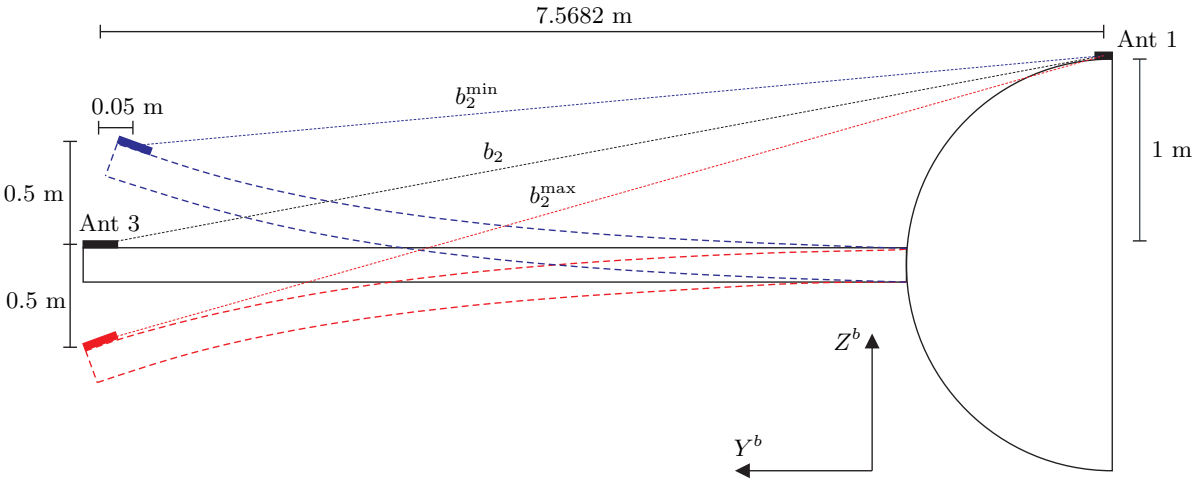

Figure B-1: Illustration of how the baseline 2 noise radius is estimated.

In Figure B-1 $b_2^{\min}$ and $b_2^{\max}$ are the min and max possible baseline lengths illustrated by the blue and red bended wing and $b_2 = 7.634$ meters. When calculating the $b_2^{\min}$ length it is assumed that a bending in the Z^b-direction of the BF reference frame of 0.5 meters will results in a bending of 0.05 meters in the Y^b-direction of the BF reference frame. This is 10% of the Z^b-direction distance and the bending ratio is the same for all other baseline noise radius estimations. For the $b_2^{\max}$ length it is assumed that there is no Y^b-direction bending of antenna 3. From Figure B-1 the min and max baseline lengths are

$$b_2^{\min} = \sqrt{(7.5682 - 0.05)^2 + 0.5^2} = 7.5348 \tag{B-1}$$

$$b_2^{\max} = \sqrt{7.5682^2 + 1.5^2} = 7.7154 \tag{B-2}$$

and the noise radiuses in percentage of b_2 are

$$100 \cdot \frac{b_2 - b_2^{\min}}{b_2} = 1.3\% \tag{B-3}$$

$$100 \cdot \frac{b_2^{\max} - b_2}{b_2} = 1.07\% \tag{B-4}$$

From Equation B-3 and B-4 the largest percentage is taken, this is further rounded up to 1.5% as many estimations where made. The baseline length noise radiuses for all other baselines are estimated in a similar way.

Appendix C

Additional Results

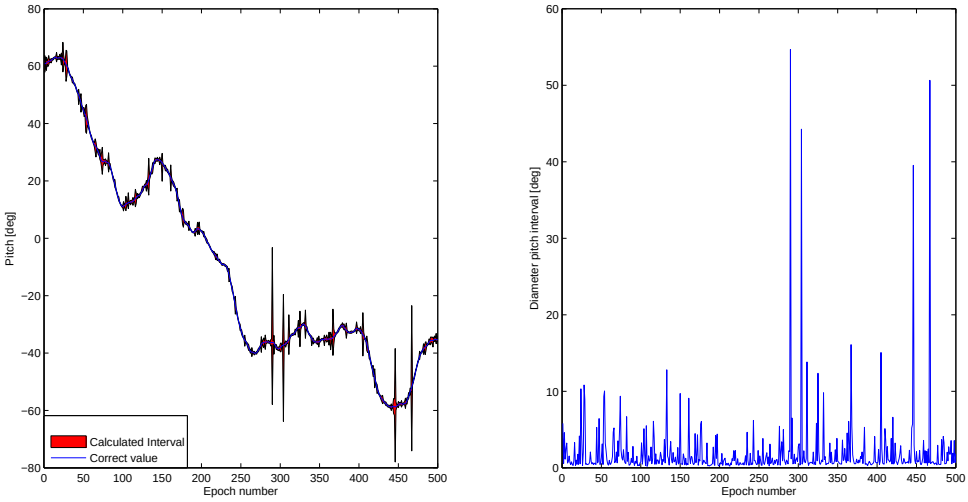

Figure C-1: Simulated pitch angle and calculated pitch interval, illustrating the problem of overestimated intervals.

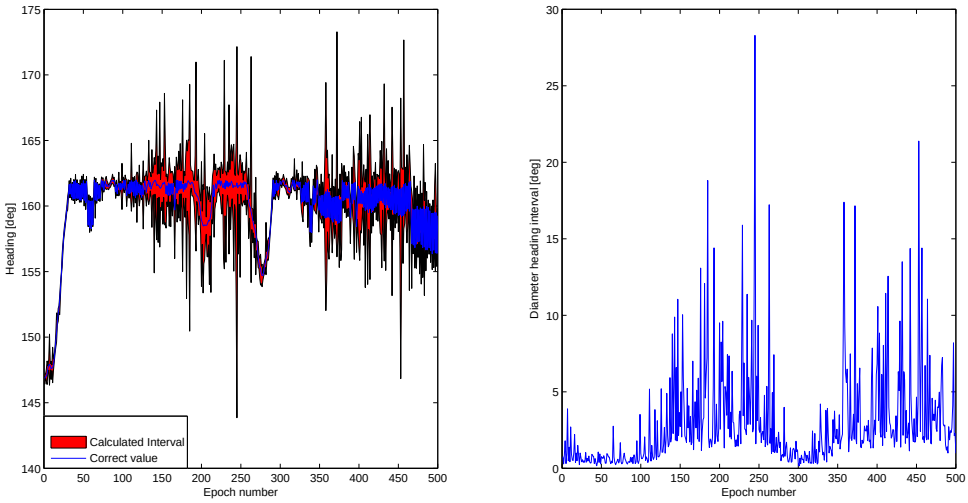

Figure C-2: Simulated heading angle and calculated heading interval, illustrating the problem of overestimated intervals.

Table C-1: Percentage of epochs containing one solution for baseline 1 and 2, NCBO and CBO, for different number of satellites in view. Tabulated for the three antenna/frequency configurations with the baseline length noise levels accordingly to Table 6-2 and the L1 and L2 carrier phase noise diameters 14 and 22.5 mm. For the 3 antenna, 1 frequency configuration the baseline noise levels are 10% of the ones in Table 6-2.

	$\mathbf{b_1}$, NCBO [%]	$\mathbf{b_2}$, NCBO [%]	$\mathbf{b_1}$, CBO [%]	$\mathbf{b_2}$, CBO [%]
3 Ant, 1 Freq, 6 Sat	0.00	0.00	0.60	0.60
3 Ant, 1 Freq, 7 Sat	2.40	0.00	92.20	89.80
3 Ant, 1 Freq, 8 Sat	52.00	0.40	99.60	98.80
3 Ant, 1 Freq, 9 Sat	87.00	36.40	100.00	100.00
3 Ant, 1 Freq, 10 Sat	95.40	78.60	100.00	100.00
3 Ant, 1 Freq, 11 Sat	98.60	93.80	100.00	100.00
Average	55.90	34.87	82.07	81.53
3 Ant, 2 Freq, 6 Sat	98.60	44.60	100.00	99.90
3 Ant, 2 Freq, 7 Sat	99.80	86.80	100.00	100.00
3 Ant, 2 Freq, 8 Sat	100.00	98.10	100.00	100.00
3 Ant, 2 Freq, 9 Sat	100.00	99.60	100.00	100.00
3 Ant, 2 Freq, 10 Sat	100.00	99.90	100.00	100.00
3 Ant, 2 Freq, 11 Sat	100.00	100.00	100.00	100.00
Average	99.73	88.17	100.00	99.98
4 Ant, 2 Freq, 6 Sat	97.90	43.00	100.00	100.00
4 Ant, 2 Freq, 7 Sat	99.70	88.40	100.00	100.00
4 Ant, 2 Freq, 8 Sat	99.90	97.90	100.00	100.00
4 Ant, 2 Freq, 9 Sat	100.00	99.60	100.00	100.00
4 Ant, 2 Freq, 10 Sat	99.90	99.80	100.00	100.00
4 Ant, 2 Freq, 11 Sat	99.90	99.90	100.00	100.00
Average	99.55	88.10	100.00	100.00

Table C-2: Min, mean and max number of solutions remaining baseline 1 and 2, NCBO, for different number of satellites in view. Tabulated for the three antenna/frequency configurations with the baseline length noise levels accordingly to Table 6-2 and the L1 and L2 carrier phase noise diameters 14 and 22.5 mm. For the 3 antenna, 1 frequency configuration the baseline noise levels are 10% of the ones in Table 6-2.

	Min $\mathbf{b_1}$	Mean $\mathbf{b_1}$	Max $\mathbf{b_1}$	Min $\mathbf{b_2}$	Mean $\mathbf{b_2}$	Max $\mathbf{b_2}$
3 Ant, 1 Freq, 6 Sat	14	33.7120	89	84	431.2240	757
3 Ant, 1 Freq, 7 Sat	1	5.1800	14	8	32.2800	104
3 Ant, 1 Freq, 8 Sat	1	1.6240	5	1	6.7060	20
3 Ant, 1 Freq, 9 Sat	1	1.1420	4	1	2.1220	7
3 Ant, 1 Freq, 10 Sat	1	1.0480	3	1	1.2540	5
3 Ant, 1 Freq, 11 Sat	1	1.0140	2	1	1.0700	3
Average		7.2867			79.1093	
3 Ant, 2 Freq, 6 Sat	1	1.0140	2	1	1.9520	12
3 Ant, 2 Freq, 7 Sat	1	1.0020	2	1	1.1450	4
3 Ant, 2 Freq, 8 Sat	1	1.0000	1	1	1.0200	3
3 Ant, 2 Freq, 9 Sat	1	1.0000	1	1	1.0040	2
3 Ant, 2 Freq, 10 Sat	1	1.0000	1	1	1.0010	2
3 Ant, 2 Freq, 11 Sat	1	1.0000	1	1	1.0000	1
Average		1.0027			1.1870	
4 Ant, 2 Freq, 6 Sat	1	1.0210	2	1	2.0440	10
4 Ant, 2 Freq, 7 Sat	1	1.0030	2	1	1.1300	4
4 Ant, 2 Freq, 8 Sat	1	1.0020	3	1	1.0230	3
4 Ant, 2 Freq, 9 Sat	1	1.0000	1	1	1.0040	2
4 Ant, 2 Freq, 10 Sat	1	1.0010	2	1	1.0020	2
4 Ant, 2 Freq, 11 Sat	1	1.0010	2	1	1.0010	2
Average		1.0047			1.2007	

Table C-3: Min, mean and max number of solutions remaining baseline 1 and 2, CBO, for different number of satellites in view. Tabulated for the three antenna/frequency configurations with the baseline length noise levels accordingly to Table 6-2 and the L1 and L2 carrier phase noise diameters 14 and 22.5 mm. For the 3 antenna, 1 frequency configuration the baseline noise levels are 10% of the ones in Table 6-2.

	Min $\mathbf{b_1}$	Mean $\mathbf{b_1}$	Max $\mathbf{b_1}$	Min $\mathbf{b_2}$	Mean $\mathbf{b_2}$	Max $\mathbf{b_2}$
3 Ant, 1 Freq, 6 Sat	1	10.3200	60	1	20.0220	562
3 Ant, 1 Freq, 7 Sat	1	1.1060	9	1	1.2080	34
3 Ant, 1 Freq, 8 Sat	1	1.0040	2	1	1.0120	2
3 Ant, 1 Freq, 9 Sat	1	1.0000	1	1	1.0000	1
3 Ant, 1 Freq, 10 Sat	1	1.0000	1	1	1.0000	1
3 Ant, 1 Freq, 11 Sat	1	1.0000	1	1	1.0000	1
Average		2.5717			4.2070	
3 Ant, 2 Freq, 6 Sat	1	1.0000	1	1	1.0010	2
3 Ant, 2 Freq, 7 Sat	1	1.0000	1	1	1.0000	1
3 Ant, 2 Freq, 8 Sat	1	1.0000	1	1	1.0000	1
3 Ant, 2 Freq, 9 Sat	1	1.0000	1	1	1.0000	1
3 Ant, 2 Freq, 10 Sat	1	1.0000	1	1	1.0000	1
3 Ant, 2 Freq, 11 Sat	1	1.0000	1	1	1.0000	1
Average		1.0000			1.0002	
4 Ant, 2 Freq, 6 Sat	1	1.0000	1	1	1.0000	1
4 Ant, 2 Freq, 7 Sat	1	1.0000	1	1	1.0000	1
4 Ant, 2 Freq, 8 Sat	1	1.0000	1	1	1.0000	1
4 Ant, 2 Freq, 9 Sat	1	1.0000	1	1	1.0000	1
4 Ant, 2 Freq, 10 Sat	1	1.0000	1	1	1.0000	1
4 Ant, 2 Freq, 11 Sat	1	1.0000	1	1	1.0000	1
Average		1.0000			1.0000	

Table C-4: Min, mean and max computation times, for different number of satellites in view. Tabulated for the three antenna/frequency configurations with the baseline length noise levels accordingly to Table 6-2 and the L1 and L2 carrier phase noise diameters 14 and 22.5 mm. For the 3 antenna, 1 frequency configuration the baseline noise levels are 10% of the ones in Table 6-2.

	Min Computation Time [s]	Mean Computation Time [s]	Max Computation Time [s]
3 Ant, 1 Freq, 6 Sat	27.8160	151.6000	507.3892
3 Ant, 1 Freq, 7 Sat	19.0764	27.7807	35.0642
3 Ant, 1 Freq, 8 Sat	20.5591	27.4545	33.0537
3 Ant, 1 Freq, 9 Sat	23.5028	31.3392	36.7379
3 Ant, 1 Freq, 10 Sat	27.5980	35.3133	41.6537
3 Ant, 1 Freq, 11 Sat	30.9378	39.9855	46.1653
Average		52.2455	
3 Ant, 2 Freq, 6 Sat	0.9666	1.4467	2.0675
3 Ant, 2 Freq, 7 Sat	1.0004	1.4147	1.9842
3 Ant, 2 Freq, 8 Sat	0.9717	1.4454	1.9464
3 Ant, 2 Freq, 9 Sat	1.1002	1.4884	1.9916
3 Ant, 2 Freq, 10 Sat	1.1449	1.5440	2.0828
3 Ant, 2 Freq, 11 Sat	1.1013	1.5980	2.2295
Average		1.4895	
4 Ant, 2 Freq, 6 Sat	2.5177	4.3854	7.0037
4 Ant, 2 Freq, 7 Sat	2.6023	3.9776	5.7180
4 Ant, 2 Freq, 8 Sat	2.6691	4.0966	6.0916
4 Ant, 2 Freq, 9 Sat	2.9382	4.2999	6.2941
4 Ant, 2 Freq, 10 Sat	3.0910	4.4727	6.4491
4 Ant, 2 Freq, 11 Sat	3.1496	4.6733	6.5307
Average		4.3176	

Table C-5: Min, mean and max number of comparisons, for different number of satellites in view. Tabulated for the three antenna/frequency configurations with the baseline length noise levels accordingly to Table 6-2 and the L1 and L2 carrier phase noise diameters 14 and 22.5 mm. For the 3 antenna, 1 frequency configuration the baseline noise levels are 10% of the ones in Table 6-2.

	Min Number Comparisons	Mean Number Comparisons	Max Number Comparisons
3 Ant, 1 Freq, 6 Sat	1	1.0000	1
3 Ant, 1 Freq, 7 Sat	1	1.0000	1
3 Ant, 1 Freq, 8 Sat	0	0.9980	1
3 Ant, 1 Freq, 9 Sat	0	0.6760	1
3 Ant, 1 Freq, 10 Sat	0	0.2480	1
3 Ant, 1 Freq, 11 Sat	0	0.0740	1
Average		0.6660	
3 Ant, 2 Freq, 6 Sat	0	0.5600	1
3 Ant, 2 Freq, 7 Sat	0	0.1330	1
3 Ant, 2 Freq, 8 Sat	0	0.0190	1
3 Ant, 2 Freq, 9 Sat	0	0.0040	1
3 Ant, 2 Freq, 10 Sat	0	0.0010	1
3 Ant, 2 Freq, 11 Sat	0	0.0000	0
Average		0.1195	
4 Ant, 2 Freq, 6 Sat	0	0.5790	1
4 Ant, 2 Freq, 7 Sat	0	0.1180	1
4 Ant, 2 Freq, 8 Sat	0	0.0220	1
4 Ant, 2 Freq, 9 Sat	0	0.0040	1
4 Ant, 2 Freq, 10 Sat	0	0.0030	1
4 Ant, 2 Freq, 11 Sat	0	0.0020	1
Average		0.1213	

Table C-6: Min, mean and max diameter pitch interval, for different number of satellites in view. Tabulated for the three antenna/frequency configurations with the baseline length noise levels accordingly to Table 6-2 and the L1 and L2 carrier phase noise diameters 14 and 22.5 mm. For the 3 antenna, 1 frequency configuration the baseline noise levels are 10% of the ones in Table 6-2.

	Min Diam Pitch Interval [deg]	Mean Diam Pitch Interval [deg]	Max Diam Pitch Interval [deg]
3 Ant, 1 Freq, 6 Sat	0.3582	0.6114	1.0093
3 Ant, 1 Freq, 7 Sat	0.2072	1.3923	29.3830
3 Ant, 1 Freq, 8 Sat	0.2142	1.4078	180.0000
3 Ant, 1 Freq, 9 Sat	0.1769	1.2752	180.0000
3 Ant, 1 Freq, 10 Sat	0.1822	0.8683	2.5380
3 Ant, 1 Freq, 11 Sat	0.1631	0.9786	2.6449
Average		1.0889	
3 Ant, 2 Freq, 6 Sat	0.1781	2.3222	180.0000
3 Ant, 2 Freq, 7 Sat	0.1634	1.9939	180.0000
3 Ant, 2 Freq, 8 Sat	0.1770	1.0241	28.2572
3 Ant, 2 Freq, 9 Sat	0.1365	0.9877	12.5415
3 Ant, 2 Freq, 10 Sat	0.1961	0.8958	2.7295
3 Ant, 2 Freq, 11 Sat	0.1757	0.9553	2.8721
Average		1.3632	
4 Ant, 2 Freq, 6 Sat	0.1283	2.4788	180.0000
4 Ant, 2 Freq, 7 Sat	0.0966	1.4337	27.0794
4 Ant, 2 Freq, 8 Sat	0.1383	1.2642	49.2321
4 Ant, 2 Freq, 9 Sat	0.1467	0.9706	36.5656
4 Ant, 2 Freq, 10 Sat	0.1501	0.9074	3.0640
4 Ant, 2 Freq, 11 Sat	0.1283	0.9641	2.1814
Average		1.3365	

Table C-7: Min, mean and max diameter heading interval, for different number of satellites in view. Tabulated for the three antenna/frequency configurations with the baseline length noise levels accordingly to Table 6-2 and the L1 and L2 carrier phase noise diameters 14 and 22.5 mm. For the 3 antenna, 1 frequency configuration the baseline noise levels are 10% of the ones in Table 6-2.

	Min Diam Heading Interval [deg]	Mean Diam Heading Interval [deg]	Max Diam Heading Interval [deg]
3 Ant, 1 Freq, 6 Sat	0.5561	2.8201	7.3219
3 Ant, 1 Freq, 7 Sat	0.2197	2.7695	44.1741
3 Ant, 1 Freq, 8 Sat	0.1972	3.2651	360.0000
3 Ant, 1 Freq, 9 Sat	0.1973	3.9476	360.0000
3 Ant, 1 Freq, 10 Sat	0.5558	4.0575	15.9760
3 Ant, 1 Freq, 11 Sat	0.3063	4.0275	9.2914
Average		3.4812	
3 Ant, 2 Freq, 6 Sat	0.1937	6.0403	360.0000
3 Ant, 2 Freq, 7 Sat	0.2497	5.9182	360.0000
3 Ant, 2 Freq, 8 Sat	0.1530	3.1455	69.2451
3 Ant, 2 Freq, 9 Sat	0.2972	3.7504	71.4141
3 Ant, 2 Freq, 10 Sat	0.1575	2.9941	12.5345
3 Ant, 2 Freq, 11 Sat	0.1933	3.1772	15.5608
Average		4.1709	
4 Ant, 2 Freq, 6 Sat	0.1271	5.6282	360.0000
4 Ant, 2 Freq, 7 Sat	0.1568	4.6878	171.1120
4 Ant, 2 Freq, 8 Sat	0.1998	4.2420	164.7717
4 Ant, 2 Freq, 9 Sat	0.2013	3.0965	141.9491
4 Ant, 2 Freq, 10 Sat	0.1668	3.2643	13.4524
4 Ant, 2 Freq, 11 Sat	0.3049	3.8939	12.4723
Average		4.1354	

Table C-8: Min, mean and max diameter bank interval, for different number of satellites in view. Tabulated for the three antenna/frequency configurations with the baseline length noise levels accordingly to Table 6-2 and the L1 and L2 carrier phase noise diameters 14 and 22.5 mm. For the 3 antenna, 1 frequency configuration the baseline noise levels are 10% of the ones in Table 6-2.

	Min Diam Bank Interval [deg]	Mean Diam Bank Interval [deg]	Max Diam Bank Interval [deg]
3 Ant, 1 Freq, 6 Sat	1.3637	3.8111	8.5387
3 Ant, 1 Freq, 7 Sat	0.2034	4.8896	85.3870
3 Ant, 1 Freq, 8 Sat	0.4998	5.2395	360.0000
3 Ant, 1 Freq, 9 Sat	0.4833	5.4811	360.0000
3 Ant, 1 Freq, 10 Sat	1.1823	5.6028	22.5053
3 Ant, 1 Freq, 11 Sat	0.3520	5.7287	11.8856
Average		5.1254	
3 Ant, 2 Freq, 6 Sat	0.2382	8.7733	360.0000
3 Ant, 2 Freq, 7 Sat	0.6960	8.7939	360.0000
3 Ant, 2 Freq, 8 Sat	0.2300	4.6671	360.0000
3 Ant, 2 Freq, 9 Sat	0.5746	5.0770	121.7099
3 Ant, 2 Freq, 10 Sat	0.4462	4.3908	17.2106
3 Ant, 2 Freq, 11 Sat	0.2044	4.4483	20.5108
Average		6.0251	
4 Ant, 2 Freq, 6 Sat	0.2512	9.6339	360.0000
4 Ant, 2 Freq, 7 Sat	0.3644	7.7460	360.0000
4 Ant, 2 Freq, 8 Sat	0.3626	6.8002	360.0000
4 Ant, 2 Freq, 9 Sat	0.5228	4.6936	360.0000
4 Ant, 2 Freq, 10 Sat	0.3248	4.4151	17.1244
4 Ant, 2 Freq, 11 Sat	0.7171	5.4548	16.7808
Average		6.4573	

Table C-9: Percentage of epochs containing one solution for baseline 1 and 2, NCBO and CBO, for different noise diameters L1 and L2 carrier phase measurements. Tabulated for the 4 antennas, 2 frequencies configuration with eight satellites in view and the baseline noise levels accordingly to Table 6-2.

	$\mathbf{b_1}$, NCBO [%]	$\mathbf{b_2}$, NCBO [%]	$\mathbf{b_1}$, CBO [%]	$\mathbf{b_2}$, CBO [%]
L1 14 mm, L2 24.5 mm	100,00	97.60	100,00	100,00
L1 16 mm, L2 28 mm	100,00	95.60	100,00	100,00
L1 18 mm, L2 31.5 mm	100,00	91.00	100,00	100,00
L1 20 mm, L2 35 mm	100,00	82.60	100,00	100,00
L1 22 mm, L2 38.5 mm	99.80	74.60	100,00	100,00
L1 24 mm, L2 42 mm	99.60	60.20	100,00	99.60
L1 26 mm, L2 45.5 mm	98.80	44.00	100,00	100,00
L1 28 mm, L2 49 mm	98.00	25.60	100,00	99.60
L1 30 mm, L2 52.5 mm	97.60	10.60	100,00	99.40
L1 32 mm, L2 56 mm	92.80	2.80	100,00	98.80
L1 34 mm, L2 59.5 mm	87.40	1.80	100,00	93.60
L1 36 mm, L2 63 mm	83.40	0.80	99.80	94.40
L1 38 mm, L2 66.5 mm	73.40	0.00	99.40	88.00
L1 40 mm, L2 70 mm	64.60	0.00	99.20	84.40

Table C-10: Min, mean and max number of solutions remaining baseline 1 and 2, NCBO, for different noise diameters L1 and L2 carrier phase measurements. Tabulated for the 4 antennas, 2 frequencies configuration with eight satellites in view and the baseline noise levels accordingly to Table 6-2.

	Min $\mathbf{b_1}$	Mean $\mathbf{b_1}$	Max $\mathbf{b_1}$	Min $\mathbf{b_2}$	Mean $\mathbf{b_2}$	Max $\mathbf{b_2}$
L1 14 mm, L2 24.5 mm	1	1,0000	1	1	1.0240	2
L1 16 mm, L2 28 mm	1	1,0000	1	1	1.0460	3
L1 18 mm, L2 31.5 mm	1	1,0000	1	1	1.1020	4
L1 20 mm, L2 35 mm	1	1,0000	1	1	1.2160	4
L1 22 mm, L2 38.5 mm	1	1.0020	2	1	1.3280	6
L1 24 mm, L2 42 mm	1	1.0040	2	1	1.6000	8
L1 26 mm, L2 45.5 mm	1	1.0120	2	1	2.1820	13
L1 28 mm, L2 49 mm	1	1.0200	2	1	3.3400	21
L1 30 mm, L2 52.5 mm	1	1.0240	2	1	4.8880	28
L1 32 mm, L2 56 mm	1	1.0780	3	1	8.5140	40
L1 34 mm, L2 59.5 mm	1	1.1360	4	1	15.0540	215
L1 36 mm, L2 63 mm	1	1.1800	4	1	34.9660	280
L1 38 mm, L2 66.5 mm	1	1.3160	5	3	96.3440	440
L1 40 mm, L2 70 mm	1	1.4640	5	4	242.8260	643

Table C-11: Min, mean and max number of solutions remaining baseline 1 and 2, CBO, for different noise diameters L1 and L2 carrier phase measurements. Tabulated for the 4 antennas, 2 frequencies configuration with eight satellites in view and the baseline noise levels accordingly to Table 6-2.

,

	Min $\mathbf{b_1}$	Mean $\mathbf{b_1}$	Max $\mathbf{b_1}$	Min $\mathbf{b_2}$	Mean $\mathbf{b_2}$	Max $\mathbf{b_2}$
L1 14 mm, L2 24.5 mm	1	1,0000	1	1	1,0000	1
L1 16 mm, L2 28 mm	1	1,0000	1	1	1,0000	1
L1 18 mm, L2 31.5 mm	1	1,0000	1	1	1,0000	1
L1 20 mm, L2 35 mm	1	1,0000	1	1	1,0000	1
L1 22 mm, L2 38.5 mm	1	1,0000	1	1	1,0000	1
L1 24 mm, L2 42 mm	1	1,0000	1	1	1.0040	2
L1 26 mm, L2 45.5 mm	1	1,0000	1	1	1.0000	1
L1 28 mm, L2 49 mm	1	1,0000	1	1	1.0040	2
L1 30 mm, L2 52.5 mm	1	1,0000	1	1	1.0060	2
L1 32 mm, L2 56 mm	1	1,0000	1	1	1.0140	3
L1 34 mm, L2 59.5 mm	1	1,0000	1	1	1.0760	5
L1 36 mm, L2 63 mm	1	1.0020	2	1	1.0740	5
L1 38 mm, L2 66.5 mm	1	1.0060	2	1	1.2060	36
L1 40 mm, L2 70 mm	1	1.0080	2	1	1.2300	7

Table C-12: Min, mean and max computation times, for different noise diameters L1 and L2 carrier phase measurements. Tabulated for the 4 antennas, 2 frequencies configuration with eight satellites in view and the baseline noise levels accordingly to Table 6-2.

	Min Computation Time [s]	Mean Computation Time [s]	Max Computation Time [s]
L1 14 mm, L2 24.5 mm	2.7651	4.0819	5.8575
L1 16 mm, L2 28 mm	3.0227	4.6080	6.6590
L1 18 mm, L2 31.5 mm	3.4937	5.5391	8.1769
L1 20 mm, L2 35 mm	4.7558	6.6499	9.0415
L1 22 mm, L2 38.5 mm	5.1111	7.3295	10.1612
L1 24 mm, L2 42 mm	5.3902	8.0385	10.9693
L1 26 mm, L2 45.5 mm	5.9017	9.2774	14.3928
L1 28 mm, L2 49 mm	6.4591	11.1865	19.6693
L1 30 mm, L2 52.5 mm	7.3337	16.4471	45.5443
L1 32 mm, L2 56 mm	8.6444	43.0596	159.1861
L1 34 mm, L2 59.5 mm	9.9997	137.2787	385.3964
L1 36 mm, L2 63 mm	11.6353	428.9220	984.4248
L1 38 mm, L2 66.5 mm	16.0710	1155.4997	2677.0310
L1 40 mm, L2 70 mm	26.6565	2427.8484	5283.1801

Table C-13: Min, mean and max number of comparisons, for different noise diameters L1 and L2 carrier phase measurements. Tabulated for the 4 antennas, 2 frequencies configuration with eight satellites in view and the baseline noise levels accordingly to Table 6-2.

	Min Number Comparisons	Mean Number Comparisons	Max Number Comparisons
L1 14 mm, L2 24.5 mm	0	0.0240	1
L1 16 mm, L2 28 mm	0	0.0440	1
L1 18 mm, L2 31.5 mm	0	0.0900	1
L1 20 mm, L2 35 mm	0	0.1740	1
L1 22 mm, L2 38.5 mm	0	0.2560	1
L1 24 mm, L2 42 mm	0	0.4180	8
L1 26 mm, L2 45.5 mm	0	0.5680	3
L1 28 mm, L2 49 mm	0	0.7820	8
L1 30 mm, L2 52.5 mm	0	0.9420	8
L1 32 mm, L2 56 mm	0	1.0740	8
L1 34 mm, L2 59.5 mm	0	1.4620	8
L1 36 mm, L2 63 mm	0	1.4360	8
L1 38 mm, L2 66.5 mm	1	1.9700	8
L1 40 mm, L2 70 mm	1	2.2480	12

Table C-14: Percentage of epochs containing one solution for baseline 1 and 2, NCBO and CBO, for different baseline length noise radius (same noise percentage all baselines). Tabulated for the 4 antennas, 2 frequencies configuration with eight satellites in view and the L1 and L2 carrier phase noise diameters 14 and 22.5 mm.

	$\mathbf{b_1}$, NCBO [%]	$\mathbf{b_2}$, NCBO [%]	$\mathbf{b_1}$, CBO [%]	$\mathbf{b_2}$, CBO [%]
Baseline length noise radius 0%	100.00	100.00	100.00	100.00
Baseline length noise radius 1%	99.80	99.80	100.00	100.00
Baseline length noise radius 2%	98.20	94.20	100.00	100.00
Baseline length noise radius 3%	95.80	76.40	100.00	100.00
Baseline length noise radius 4%	86.60	54.00	100.00	100.00

Table C-15: Min, mean and max number of solutions remaining baseline 1 and 2, NCBO, for different baseline length noise radius (same noise percentage all baselines). Tabulated for the 4 antennas, 2 frequencies configuration with eight satellites in view and the L1 and L2 carrier phase noise diameters 14 and 22.5 mm.

	Min $\mathbf{b_1}$	Mean $\mathbf{b_1}$	Max $\mathbf{b_1}$	Min $\mathbf{b_2}$	Mean $\mathbf{b_2}$	Max $\mathbf{b_2}$
Baseline length noise radius 0%	1	1.0000	1	1	1.0000	1
Baseline length noise radius 1%	1	1.0020	2	1	1.0020	2
Baseline length noise radius 2%	1	1.0200	3	1	1.0600	3
Baseline length noise radius 3%	1	1.0500	4	1	1.3040	6
Baseline length noise radius 4%	1	1.1720	6	1	2.0860	29

Table C-16: Min, mean and max number of solutions remaining baseline 1 and 2, CBO, for different baseline length noise radius (same noise percentage all baselines). Tabulated for the 4 antennas, 2 frequencies configuration with eight satellites in view and the L1 and L2 carrier phase noise diameters 14 and 22.5 mm.

	Min $\mathbf{b_1}$	Mean $\mathbf{b_1}$	Max $\mathbf{b_1}$	Min $\mathbf{b_2}$	Mean $\mathbf{b_2}$	Max $\mathbf{b_2}$
Baseline length noise radius 0%	1	1,0000	1	1	1.0000	1
Baseline length noise radius 1%	1	1,0000	1	1	1.0000	1
Baseline length noise radius 2%	1	1,0000	1	1	1.0000	1
Baseline length noise radius 3%	1	1,0000	1	1	1.0000	1
Baseline length noise radius 4%	1	1,0000	1	1	1.0000	1

Table C-17: Min, mean and max computation times, for different baseline length noise radius (same noise percentage all baselines). Tabulated for the 4 antennas, 2 frequencies configuration with eight satellites in view and the L1 and L2 carrier phase noise diameters 14 and 22.5 mm.

	Min Computation Time [s]	Mean Computation Time [s]	Max Computation Time [s]
Baseline length noise radius 0%	2.6281	3.8553	5.2568
Baseline length noise radius 1%	2.8538	4.2294	6.0860
Baseline length noise radius 2%	3.6313	6.7327	13.1336
Baseline length noise radius 3%	5.1874	604.9107	1541.4984
Baseline length noise radius 4%	6.3528	2837.8927	7213.8609

Table C-18: Min, mean and max number of comparisons, for different baseline length noise radius (same noise percentage all baselines). Tabulated for the 4 antennas, 2 frequencies configuration with eight satellites in view and the L1 and L2 carrier phase noise diameters 14 and 22.5 mm.

	Min Number Comparisons	Mean Number Comparisons	Max Number Comparisons
Baseline length noise radius 0%	0	0.0000	0
Baseline length noise radius 1%	0	0.0040	1
Baseline length noise radius 2%	0	0.0740	1
Baseline length noise radius 3%	0	0.2720	1
Baseline length noise radius 4%	0	0.5340	3